TKK Dissertations 173
Espoo 2009

EXPANDING THE APPLICABILITY OF MAGNETOENCEPHALOGRAPHY

Doctoral Dissertation

Lauri Parkkonen

Helsinki University of Technology
Low Temperature Laboratory

Helsinki University of Technology
Faculty of Information and Natural Sciences
Department of Biomedical Engineering and Computational Science

TKK Dissertations 173
Espoo 2009

EXPANDING THE APPLICABILITY OF MAGNETOENCEPHALOGRAPHY

Doctoral Dissertation

Lauri Parkkonen

Dissertation for the degree of Doctor of Science in Technology to be presented with due permission of the Faculty of Information and Natural Sciences for public examination and debate in Auditorium AS2 at Helsinki University of Technology (Espoo, Finland) on the 12th of June, 2009, at 12 noon.

Helsinki University of Technology
Low Temperature Laboratory

Teknillinen korkeakoulu
Kylmälaboratorio

Helsinki University of Technology
Faculty of Information and Natural Sciences
Department of Biomedical Engineering and Computational Science

Teknillinen korkeakoulu
Informaatio- ja luonnontieteiden tiedekunta
Lääketieteellisen tekniikan ja laskennallisen tieteen laitos

Distribution:
Helsinki University of Technology
Low Temperature Laboratory
Brain Research Unit
P.O. Box 5100
FI - 02015 TKK
FINLAND
URL: http://ltl.tkk.fi/
Tel. +358-9-451 5619
Fax +358-9-451 2969
E-mail: lauri@neuro.hut.fi

ISBN 978-951-22-9950-8
ISBN 978-951-22-9951-5 (PDF)
ISSN 1795-2239
ISSN 1795-4584 (PDF)
URL: http://lib.tkk.fi/Diss/2009/isbn9789512299515/

TKK-DISS-2619

Picaset Oy
Helsinki 2009

ABSTRACT OF DOCTORAL DISSERTATION	HELSINKI UNIVERSITY OF TECHNOLOGY P. O. BOX 1000, FI-02015 TKK http://www.tkk.fi

Author Lauri Parkkonen

Name of the dissertation

Expanding the applicability of magnetoencephalography

Manuscript submitted 2009-04-21	Manuscript revised 2009-05-27
Date of the defence 2009-06-12	
☐ Monograph	☒ Article dissertation (summary + original articles)

Faculty	Information and Natural Sciences
Department	Biomedical Engineering and Computational Science
Field of research	Engineering Physics, Biomedical Engineering
Opponent(s)	Prof. Shinya Kuriki
Supervisor	Prof. Risto Ilmoniemi
Instructor	Prof. Riitta Hari

Abstract

Magnetoencephalography (MEG) offers a unique way to non-invasively monitor the neural activity in the human brain. MEG is based on measuring the very weak magnetic fields generated by the electric currents in the active neurons. Such measurements allow, with certain limitations, estimating the underlying current distribution and thus the locations and time courses of the neural generators with an excellent temporal resolution.

The aim of this Thesis was to advance MEG to certain realms that have been considered difficult or even impossible for it. Specifically, the included studies contributed to the modelling of the neural generators, detection of activity in the deep brain areas, analysis of oscillatory activity, and characterisation of neural states related to bistable perception.

Estimating the sources of MEG signals is non-trivial as multiple current constellations can give rise to the same observed magnetic fields. As a new solution to this problem, we introduced an automatic Bayesian tracking algorithm that recovers the locations and time courses of a set of focal neural current sources from MEG data.

The majority of MEG experiments have concentrated on brain signals originating in the neocortex due to the rapid decrease of the MEG signals as a function increasing source depth. Here, we demonstrated that neural activity deep in the brainstem can be detected and accurately localised by MEG in favourable conditions.

We also explored the utility of stochastic resonance in varying the salience of a cognitive stimulus, and showed that the detection accuracy of visually-presented words correlated better with the amplitudes of the late than early responses.

The temporal resolution provided by MEG was exploited in novel ways. We showed that oscillatory 20-Hz signals from the primary and secondary somatosensory cortex were transiently phase-locked in response to a stimulus, possibly signifying functional connectivity. We also introduced a frequency-tagging method employing dynamical noise to separate brain activations elicited by different parts of a visual scene: monitoring these rhythmic signals with MEG enabled us to probe the neural engagement in the early visual brain areas during bistable perception and thus to link subjective perceptual states to brain states.

Keywords	magnetoencephalography, signal processing, inverse modelling, brain, human sensory systems
ISBN (printed) 978-951-22-9950-8	ISSN (printed) 1795-2239
ISBN (pdf) 978-951-22-9951-5	ISSN (pdf) 1795-4584
Language English	Number of pages 88 + 52 in Appendices
Publisher	Low Temperature Laboratory, Helsinki University of Technology
Print distribution	Low Temperature Laboratory, Helsinki University of Technology
☒ The dissertation can be read at http://lib.tkk.fi/Diss/2009/isbn9789512299515/	

VÄITÖSKIRJAN TIIVISTELMÄ	TEKNILLINEN KORKEAKOULU PL 1000, 02015 TKK http://www.tkk.fi

Tekijä Lauri Parkkonen

Väitöskirjan nimi

Magnetoenkefalografian sovellusalueen laajennoksia

Käsikirjoituksen päivämäärä 2009-04-21	Korjatun käsikirjoituksen päivämäärä 2009-05-27
Väitöstilaisuuden ajankohta 2009-06-12	
☐ Monografia	☒ Yhdistelmäväitöskirja (yhteenveto + erillisartikkelit)

Tiedekunta	Informaatio- ja luonnontieteiden tiedekunta
Laitos	Lääketieteellisen tekniikan ja laskennallisen tieteen laitos
Tutkimusala	Teknillinen fysiikka, lääketieteellinen tekniikka
Vastaväittäjä(t)	Prof. Shinya Kuriki
Työn valvoja	Prof. Risto Ilmoniemi
Työn ohjaaja	Prof. Riitta Hari

Tiivistelmä

Magnetoenkefalografia (MEG) tarjoaa turvallisen tavan tutkia ihmisaivojen toimintaa. MEG perustuu aktiivisissa hermosoluissa kulkevien sähkövirtojen synnyttämien heikkojen magneettikenttien mittaamiseen pään ulkopuolella. Näistä mittauksista voidaan tietyin rajoituksin päätellä magneettikentät synnyttänyt virtajakauma ja siten aktiivisten aivoalueiden paikat ja niiden aktiivisuuden muutokset ajassa.

Tässä väitöskirjassa kehitettiin menetelmiä MEG:n soveltamiseksi sellaisillekin tutkimusalueille, joita on aiemmin pidetty sille vaikeina tai jopa mahdottomina. Väitöskirjan osatöissä esiteltiin uusia menetelmiä aktiivisten alueiden mallintamiseksi, syvien aivoalueiden toiminnan mittaamiseksi, rytmisen aivotoiminnan analysoimiseksi ja vaihduntakuvioiden havainnointiin liittyvien hermostollisten tilojen kartoittamiseksi.

Aktiivisten aivoalueiden estimointi MEG-mittauksista on vaikeaa, sillä useat virtajakaumat voivat synnyttää samanlaisen kenttäjakauman. Kehitimme bayesiläiseen seurantaan perustuvan menetelmän, joka pystyy automaattisesti rekonstruoimaan MEG-mittauksista usean neuraalisen lähteen paikat ja aikakäyttäytymiset.

Valtaosassa MEG-kokeista tutkitaan aivokuorella syntyneitä nopeita vasteita ja rytmistä toimintaa, sillä näistä syntyvät signaalit näkyvät MEG:llä parhaiten. Tässä työssä osoitimme, että myös syvien aivorakenteiden, erityisesti aivorungon tuottamia signaaleita voidaan mitata MEG:llä ja niiden lähteet voidaan paikantaa suotuisissa olosuhteissa.

Tutkimme myös stokastisen resonanssin käyttöä näköärsykkeessä ja osoitimme, että sanoille syntyvien myöhäisten aivovasteiden voimakkuus korreloi tunnistustarkkuuden kanssa paremmin kuin aikaisempien vasteiden voimakkuus.

Käytimme hyväksi MEG:n erinomaista ajallista tarkkuutta uusilla tavoilla. Osoitimme että ihmisen primaarisen ja sekundaarisen tuntoaivokuoren tuottamat MEG-signaalit vaihelukittuvat hetkellisesti osana tuntoärsykkeen käsittelyä. Kehitimme myös taajuusmerkintää ja kohinaa käyttävän menetelmän joka mahdollisti ihmisen näköjärjestelmän tutkimisen uudella tavalla: pystyimme MEG:n avulla seuraamaan näköaivokuoren toimintaa ja osoittamaan, että vaihduntakuvion näköhavainnon muuttumiseen liittyy vastaava aktivaatiomuutos jo varhaisilla näköalueilla.

Asiasanat	magnetoenkefalografia, signaalinkäsittely, käänteismallinnus, aivotutkimus, ihmisen aistijärjestelmät
ISBN (painettu) 978-951-22-9950-8	ISSN (painettu) 1795-2239
ISBN (pdf) 978-951-22-9951-5	ISSN (pdf) 1795-4584
Kieli Englanti	Sivumäärä 88 + 52 liitteinä.
Julkaisija	Kylmälaboratorio, Teknillinen korkeakoulu
Painetun väitöskirjan jakelu	Kylmälaboratorio, Teknillinen korkeakoulu
☒ Luettavissa verkossa osoitteessa http://lib.tkk.fi/Diss/2009/isbn9789512299515/	

Academic dissertation

Expanding the Applicability of Magnetoencephalography

Author	Lauri Parkkonen Low Temperature Laboratory, Brain Research Unit Helsinki University of Technology Finland
Supervising professor	Prof. Risto Ilmoniemi Department of Biomedical Engineering and Computational Science Helsinki University of Technology Finland
Supervisor	Prof. Riitta Hari Low Temperature Laboratory, Brain Research Unit Helsinki University of Technology Finland
Preliminary examiners	Prof. Seppo P. Ahlfors Athinoula A. Martinos Center for Biomedical Imaging Massachusetts General Hospital Harvard University United States of America
	Prof. Bernd Lütkenhöner HNO Klinik, Department of Experimental Audiology University of Münster Germany
Official opponent	Prof. Shinya Kuriki Research Center for Advanced Technologies Tokyo Denki University Japan

Contents

Contents ix

List of Publications xi

Author's contribution xiii

List of Abbreviations xv

Preface and acknowledgements xvii

1 Introduction 1

2 Background 3

2.1 Origin of neuromagnetic signals 4

2.1.1 Neural signalling 4

2.1.2 Neural currents 6

2.2 Instrumentation for magnetoencephalography 8

2.2.1 Signal strength 8

2.2.2 Sensors and systems 10

2.2.3 Interference suppression 12

2.3 Signal processing 15

2.3.1 Averaging and filtering 15

2.3.2 Extracting oscillatory responses from MEG data 16

2.3.3 Phase-locking analysis 22

2.4 Source modelling 23

2.4.1 From neural currents to magnetic fields 24

2.4.2 From magnetic fields to neural currents 29

2.4.3 Post-processing and visualisation 34

3 Objectives 37

4 Summary of studies 39

4.1 Methods 39

4.1.1 Subjects 39

4.1.2 Recordings 39

4.1.3 MRIs and co-registration 40
4.1.4 Signal processing 41
4.1.5 Source modelling 41
4.2 Dynamical MEG source modelling (P1) 42
4.3 Magnetic auditory brainstem responses (P2) 44
4.4 Phase locking between primary and secondary somatosensory cortices (P3) 46
4.5 Stochastic resonance in visual stimulation (P4) 47
4.6 Frequency-tagging approach to study bistable visual perception (P5) . . 48

5 Discussion **51**
5.1 Benefits of spatio-temporal approaches 51
5.2 Expanding the frequency regime 52
5.3 Employing temporally-structured stimuli 54
5.4 Clinical and neuroscientific implications 55
5.5 Future directions 56

6 Conclusions **57**

References **59**

List of Publications

This Thesis comprises a summary and the following publications, referred to in the text as P1–P5.

P1 Sorrentino A, **Parkkonen L**, Pascarella A, Campi C, Piana M (2009). Dynamical MEG source modeling with multi-target Bayesian filtering. *Hum Brain Mapp* 30: 1911–1921.

P2 **Parkkonen L**, Fujiki N, Mäkelä JP (2009). Sources of auditory brainstem responses revisited: Contribution by magnetoencephalography. *Hum Brain Mapp* 30: 1772–1782.

P3 Simões C, Jensen O, **Parkkonen L**, Hari R (2003). Phase-locking between human SI and SII cortices. *Proc Natl Acad Sci U S A* 100: 2691–2694.

P4 Sorrentino A, **Parkkonen L**, Piana M, Massone AM, Narici L, Carozzo S, Riani M, Sannita WG (2006). Modulation of brain and behavioural responses to cognitive visual stimuli with varying signal-to-noise ratios. *Clin Neurophysiol* 117: 1098–1105.

P5 **Parkkonen L**, Andersson J, Hämäläinen M, Hari R (2008). Early visual brain areas reflect the percept of an ambiguous scene. *Proc Natl Acad Sci U S A* 105: 20500–20504.

Author's contribution

In P1, I participated in devising the inverse modelling algorithm introduced in this publication, performed the MEG measurement, analysed the acquired MEG data, reviewed the results obtained with simulated data, and co-wrote the manuscript with A.S. I conceived the experiment and collected the data with the other authors in P2, analysed the data, and co-wrote the manuscript with J.M. In P3, I participated in the data analysis and commented the manuscript. I contributed to the design of the experiment in P4, conducted the measurements together with the other authors, had a major role in the data analysis and co-wrote the manuscript with A.S. and M.P. In P5, I designed the experiment with R.H., performed the measurements with J.A., analysed the data with help from J.A., M.H. and R.H., and wrote the manuscript with contributions from R.H. and M.H.

List of Abbreviations

ABR	auditory brainstem response
AEF	auditory evoked field
AP	action potential
BEM	boundary element model / method
CAP	compound action potential
dSPM	dynamic statistical parametric map / mapping
ECD	equivalent current dipole
EEG	electroencephalography
EOG	electro-oculogram
FFT	fast Fourier transform
FT	Fourier transform
fMRI	functional MRI
FWHM	full-width at half maximum
GLM	general linear model
mABR	magnetic ABR
MCE	minimum current estimate
MEG	magnetoencephalography
MNE	minimum norm estimate / estimation
MRI	magnetic resonance imaging
PCA	principal component analysis
PLF	phase-locking factor
PLS	phase-locking statistics
PLV	phase-locking value
RMS	root-mean-square
SEF	somatosensory evoked field
SI	primary somatosensory cortex
SII	secondary somatosensory cortex
SNR	signal-to-noise ratio
SQUID	superconducting quantum interference device
SR	stochastic resonance
SSP	signal-space projection
SSS	signal-space separation
STFT	short-time Fourier transform

VEF	visual evoked field
V1	primary visual cortex
V*n*	visual cortex *n*

Preface and acknowledgements

The work for this Thesis, including the magnetoencephalographic data collection, was carried out in the Brain Research Unit of the Low Temperature Laboratory at the Helsinki University of Technology (TKK). Magnetic resonance images were obtained at the Advanced Magnetic Imaging Centre of TKK and at the Department of Radiology, Helsinki University Central Hospital. The Academy of Finland (National Centers of Excellence Programmes), the Finnish Cultural Foundation, and the Sigrid Jusélius Foundation supported the work financially. The Finnish Graduate School of Neuroscience (FGSN) offered valuable learning opportunities as well as supported travelling.

The Low Temperature Laboratory provided the whole scientific environment, with excellent experimental facilities. I was privileged to work in this truly high-level scientific establishment both during the era of its founder, late Academician Olli V. Lounasmaa, and under the current director, Prof. Mikko Paalanen.

I am most thankful to Prof. Riitta Hari, both as the head of the Brain Research Unit of the Laboratory and as the supervisor of this Thesis, for letting me work in her team and for her indispensable scientific insight and guidance in the course of this project. A person with such a broad range of interests and skills is a rarity indeed.

I am indebted to Prof. Matti Hämäläinen for his multiple instrumental roles in my work. He has been a mentor and colleague since my entry into this exciting field many years ago, a member of my FGSN follow-up group, and a collaborator. Prof. Jouko Lampinen as the other member of the follow-up group, and Prof. Risto Ilmoniemi as the supervising professor have both been very supportive and encouraging throughout the project.

Research is mostly team work, and the studies comprising this Thesis are no exception. Docent Jyrki Mäkelä and Dr. Nobuya Fujiki, with their expertise ranging from the lab to the clinic, added substantial value to this work. The Genovese inverse modellers, Prof. Michele Piana, Dr. Alberto Sorrentino, Dr. Annalisa Pascarella, and M.Sc. Cristina Campi brought in many fresh ideas from their field and created an enjoyable model of team work. The other Italian collaborators, Dr. Simone Carozzo, Dr. Anna Maria Massone, Prof. Livio Narici, Prof. Massimo Riani, and Prof. Walter Sannita, also enriched this work significantly. Drs. Jesper Andersson, Ole Jensen, and Cristina Simões-Franklin have been the most wonderful people to work with, both professionally and personally. I

am grateful to all these people, for without their interest and investment in this research, the studies in this Thesis would not have been possible.

The preliminary examiners, Prof. Seppo Ahlfors and Prof. Bernd Lütkenhöner, meticulously read the manuscript and helped improve the clarity of expression. I am most grateful for their time and valuable comments.

The Brain Research Unit has always hosted a number talented individuals, and I have received help from many of them. I would like to thank Acad. Prof. Riitta Salmelin for her editorial considerations and insightful comments on my manuscripts, Docent Simo Vanni and Dr. Topi Tanskanen for intriguing discussions on the workings of the visual system and for comments on my manuscripts. I am also very grateful to Dr. Mika Seppä for kindly helping me in countless ways, with the MRIs in particular, and to MD Linda Stenbacka for sharing the famous "Linda simulations". Many thanks indeed go to Dr. Cathy Nangini, who has kept an eye on my English while also following the logic of the content of this Thesis. Docent Veikko Jousmäki has been invaluable in managing the MEG environment. Dr. Jan Kujala, Phil.Lic. Jaana Hiltunen, and M.Sc. Veli-Matti Saarinen have provided me with their expertise when it has come to computing, fibre tracing and eye tracking. Ms. Mia Illman, Mr. Jari Kainulainen, and Ms. Marita Kattelus have helped crucially by assisting in the collection of the MEG and MRI data. The dynamic IT support team of Mr. Petteri Räisänen and Mr. Ronny Schreiber has really kept things running without a hitch, the professional secretariat has ensured that the practicalities have always gone smoothly, and the helpful people at the machine and electronics workshops have made it possible to build unique experimental setups.

The importance of my parallel alma mater of the MEG method, Neuromag Oy, from the time of the "Seven Brothers" to today's full-blown research, development, and marketing departments, cannot be overestimated. I am particularly grateful to Docent Antti Ahonen for his support and willingness to create this kind of a link between the industry and academia. M.Sc. Matti Kajola, Docent Jukka Knuutila, M.Sc. Petteri Laine, Docent Jukka Nenonen, Dr. Juha Simola, and Dr. Samu Taulu with their profound understanding of the methodology have been an indispensable resource on both sides of the field. And the after-sales team has timely helped keep the instrument running.

Certain apologies are in order, too. The nice, innocent individuals, the newly-born master of science Liisa Helle, M.Sc. Miiu Kujala, M.Sc. Hannu Laaksonen, M.Sc. Pavan Ramkumar, and MD Linda Stenbacka have had the dubious honour of sharing an office

with me, and thus being distracted by the countless MEG support phone calls and office visitors. Thank you for putting up with that, and for the nice company over the years.

The social atmosphere in the lab has been remarkably enjoyable, and all the people in the BRU are to be held responsible for that. There are way too many to list, but—in addition to several of the people above—I am particularly grateful for the friendship, support, and scientific insights of Drs. Erika Kirveskari, Tiina Parviainen, Hanna Renvall, and Topi Tanskanen. The many scientific and non-scientific conversations as well as common projects with Doc. Nina Forss, Dr. Päivi Helenius, M.Sc. Annika Hultén, Dr. Miika Koskinen, MD Satu Lamminmäki, M.Sc. Mia Liljeström, Doc. Elina Pihko, and Dr. Kimmo Uutela have been most enjoyable. Several past members of the lab as well as a number of short- and long-term visitors have left an imprint at least on me, and probably also on the whole lab. Friends and collaborators in other labs, Docent Minna Huotilainen, Prof. Aapo Hyvärinen, Docent Teemu Rinne, Docent Ricardo Vigário, and the good people in the Biomag lab, have had a great positive influence.

Equally important as all the above for this work has been the time with my parents, with Eero, Elina, Noora, Olavi, and the Karhunen family at various nice locations throughout the country and on the sea. My parents Leena and Heikki have supported and helped me in a number of ways during this project, particularly by providing very flexible childcare services.

I dedicate this work to Eeva, Tapio, and Aino, who had to make an investment—whether they wanted to or not—as this work has clearly taken time that I should have spent with the family. This project has consolidated their top priority in my life.

Espoo, early June, 2009

The author

1 Introduction

Being the organ of the mind, the brain is an intriguing target of study in many scientific disciplines. The intense research on the human brain has provided us with a wealth of neuroscientific knowledge, but it has also come to ascertain the complexity of the brain. The estimated 10^{14} connections—roughly 1000 times more numerous than stars in our Galaxy—between nerve cells, the chemical processes involved, and the dynamical nature of the structure and function of the brain warrant its status as the most complex organ. This multidimensionality calls for several research methods as no single approach can fully characterise the brain, neither its function nor its structure.

Brain function can be studied from the level of single nerve cells to human behaviour. Bridging this gap appears intractable, and research able to cross several of the levels in-between is still rare. Between those extrema lies the systems-level approach to brain function. There, the activity of large cell assemblies and its relation to cognitive functions are at the primary focus rather than individual nerve cells, or neurons. Even within that niche, several methods exist for learning about the underlying brain processes. Non-invasively, one can obtain information about brain activation by monitoring the metabolism and hemodynamics in the nervous tissue. One can also record the electric signalling between neurons as manifested in extracranial electric potentials and magnetic fields. Measuring these physical quantities and inferring some characteristics of the underlying brain activity is referred to as electroencephalography (EEG) and magnetoencephalography (MEG). The virtue of these techniques is that they tap the neural processes directly in the sense that the same physical events that allow neurons to convey information are also responsible for generating these extracranial fields. By contrast, methods based on local hemodynamics, such as functional magnetic resonance imaging (fMRI) and optical imaging, monitor the activity indirectly and exhibit relatively poor temporal resolution since blood oxygenation level only sluggishly tracks neural activity.

MEG has been applied to a number of neuroscientific and clinical questions during its relatively brief history as a full-fledged research tool. In basic research, MEG has been instrumental in the study of, e.g., the human auditory, somatosensory and visual systems, as well as oscillatory brain activity. Important results have also been obtained in studies of language comprehension and production as well as of the human mirror-neuron system; for reviews, see e.g. Näätänen *et al.* (1994), Hari and Salmelin (1997), Hämäläinen and Hari (2002), Lu and Kaufman (2003), Hari and Nishitani (2004), and Salmelin (2007).

In clinical use, the main applications of MEG are in epilepsy (first indications by Barth *et al.*, 1982; a recent comparison study by Iwasaki *et al.*, 2005) and preoperative mapping of eloquent cortical areas (for the current state, see e.g. Mäkelä *et al.*, 2006).

Many of the early approaches in designing MEG experiments and analysing data are still in use; however, MEG can benefit from advances in many disciplines, including signal analysis and mathematical modelling. This Thesis is about enlarging the scope of research that could be addressed with MEG.

This summary first reviews the neurophysiological and methodological background relevant for the studies comprising the Thesis, providing links to the pertinent literature. The Background Section explains the physiological facts important for understanding the genesis and interpretation of MEG signals as well as the physics and mathematics required in processing and modelling those signals; for the general neuroscientific background, the reader is referred to the textbooks by, e.g., Kandel *et al.* (2000), Purves *et al.* (2004), and Mountcastle (1998). Thereafter, the specific aims of the Thesis are listed, and the studies are briefly summarised, followed by a general discussion on the results.

2 Background

The studies constituting this Thesis employ MEG as a means to non-invasively obtain data about the neural processes in the human brain. The excellence of MEG lies in its high temporal resolution, down to sub-milliseconds as shown in Study P2, combined with a reasonable spatial localisation power. This combination is unique. MEG's electric counterpart, EEG, features similar temporal resolution but an inferior ability to localise the sources of the signals. On the other hand, the hemodynamic measures of brain activity, positron emission tomography (PET) and fMRI, yield a spatially more accurate reconstruction of the activity but lack the millisecond-range temporal information. A combination of these methods in estimating the neural activity (see e.g. Dale *et al.*, 2000; Ahlfors and Simpson, 2004; Furey *et al.*, 2006) would, in principle, enable high spatial and temporal resolution; however, such a fusion is not straightforward as the hemodynamic (fMRI and PET) and electrophysiological (MEG and EEG) methods monitor the neural processes in very different ways and thus convey somewhat different pictures of the activity (Furey *et al.*, 2006; Liljeström *et al.*, 2009).

Using MEG or EEG is not only about the mere measurement of the signals associated with neural activity, but also entails signal processing to extract the signal components of interest. Source modelling methods are needed to move from a sensor-level description of the data to the source level, i.e., to mathematically describe the data in terms of neural generators rather than illustrating them as waveforms at the sensors. However, the problem of modelling these generators is ill-posed; multiple different source current patterns can give rise to the same MEG and EEG data. This ambiguity calls for modelling that establishes a unique solution by imposing physiologically sound constraints. Since there is room for specifying different sets of constraints that all carry some physiological validity, a number of modelling approaches have emerged in the course of the history of MEG and modern EEG.

Structural information about the human brain—obtained typically with magnetic resonance imaging (MRI)—can provide justified constraints for modelling the MEG sources; for example, the source currents can be restricted to lie only in the brain tissues that are known to be able to generate MEG activity. In addition, anatomical images can be employed in the visualisation of MEG results.

This Section introduces the basic mechanisms of neural signalling, concisely reviews the

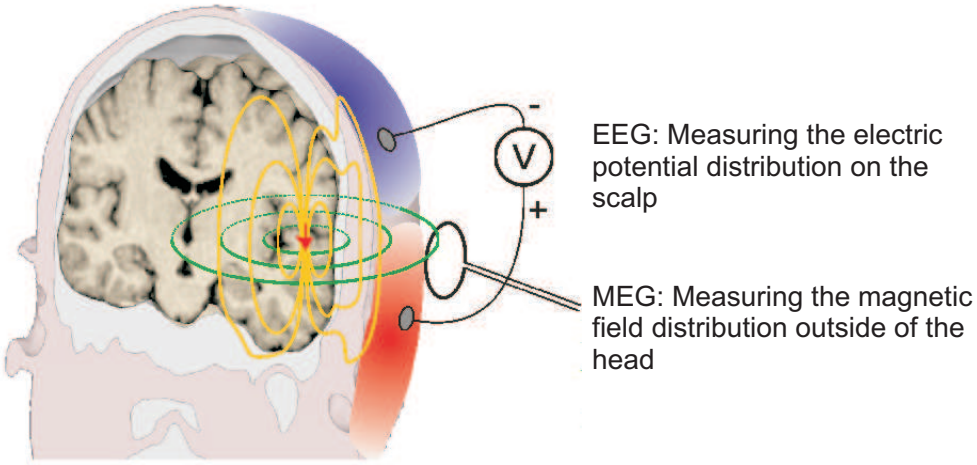

Figure 2.1 An electrically active neuron population (red arrow) gives rise to scalp potentials (red and blue shadings) and extracranial magnetic fields (green lines). Recording the scalp potentials is known as electroencephalography (EEG), and measuring the magnetic field as magnetoencephalography (MEG). Both MEG and EEG convey information about synchronised electric activity in the brain. *Background image courtesy of Mika Seppä.*

basics of the genesis of MEG and EEG signals, describes the signal processing techniques central to the studies in this Thesis, introduces the MEG source modelling problem and the ways utilised and developed in this Thesis to tackle it. Finally, the combination of MEG and structural MRI is briefly discussed.

2.1 Origin of neuromagnetic signals

2.1.1 Neural signalling

For information transfer, the human nervous system employs a combination of electrical and chemical mechanisms. Electric impulses travel faster than chemical, and they require only a conducting medium for propagation. On the other hand, with respect electric signalling, chemical transmission between cells allows them to be decoupled for independent metabolism, growth and migration. Chemical signals are also convenient in modulating the activity of the nerve cells at a slow but large scale.

A nerve cell, or neuron, comprises a tree of *dendrites* that receive information from other neurons, a cell body or *soma* where the nucleus resides, and an *axon* that conveys the out-

put of that cell to other neurons. The axon of one neuron and the dendrite of another form a contact at a *synapse*, where information is transferred usually chemically although also electrical synapses exist. A single cortical pyramidal neuron can receive input through hundreds of synapses.

Specialised proteins within the cell membrane act as *ion pumps* that actively move certain ion species across the cell membrane. These pumps maintain a high potassium and low sodium and chloride concentration within the cell with respect to the extracellular fluid. These concentration gradients and the membrane permeabilities of the ion species set up a transmembrane potential of $E_\mathrm{m} \approx -70$ mV (the inside of the cell is negative with respect to the extracellular fluid) under physiological conditions.

In a synapse, neurotransmitter molecules arriving at the post-synaptic membrane open *ion channels* that selectively let specific ion species flow passively along the concentration gradient and thus alter the transmembrane potential. An *excitatory* synapse depolarises the cell membrane locally (raises the potential to a less negative value) and thus gives rise to an *excitatory postsynaptic potential* (EPSP). By contrast, an *inhibitory* synapse hyperpolarises the cell (lowers the potential) and generates an *inhibitory postsynaptic potential* (IPSP), or shunts the membrane potential to its resting value so that simultaneous excitation is less likely to depolarise the cell.

The simultaneous excitatory and inhibitory contributions of the synapses, weighted by several factors including the distance from the soma, sum together, and this net effect determines how much the membrane potential deviates from the resting level at the soma. If the potential E_m exceeds approximately -55 mV at the root of the axon, called the *axon hillock*, an *action potential* (AP) is initiated. The distributions of excitatory and inhibitory synapses within the dendritic tree are rather different; most inhibitory synapses are located close to the soma where they influence the potential of the soma more than the excitatory synapses which are concentrated further away, at *dendritic spines*, which are small protrusions of the dendritic shaft. The dendrites contain voltage-gated channels that may amplify the effects of the post-synaptic potentials by producing *dendritic spikes*.

While EPSPs and IPSPs are graded potentials, the AP is an all-or-none event. The propagation of the AP along the axon is active; voltage-gated sodium channels open at the front of the AP wave and depolarise the membrane further up to $E_\mathrm{m} \approx +35$ mV, followed by a delayed opening of potassium channels that brings the potential down towards the resting level. This chain of events takes about 1–2 ms, after which the neuron continues

to be in a refractory state for about a millisecond during which new APs can not be fired. Normally, the AP traverses from the axon hillock to the pre-synaptic terminals. At these terminals, the AP triggers a cascade that leads to the release of neurotransmitter vesicles to the synaptic cleft where they diffuse to the receptors at the post-synaptic membrane.

The active propagation and binary nature ensure that AP can travel unchanged over long distances. However, the velocity is limited by the kinetics of the ion channels and the leakage of the intracellular current through the cell membrane. In addition, active propagation is energy-demanding. Therefore, most axons are surrounded by an electric insulator, *myelin*, which is a specialised glial cell that wraps around the axon. Myelin increases the resistance between the inside of the cell and the surroundings, and thus reduces the leakage. As a result, within a myelinated segment, the propagation of the AP is passive but fast, and between the segments, at the *nodes of Ranvier*, the propagation is active and the AP amplitude is restored. This saltatory conduction in thick, myelinated peripheral axons can reach velocities in excess of 50 m/s. In Study P2 of this Thesis, the localisation and timing obtained by MEG allowed us to estimate the conduction velocity along a part of the auditory pathway to be about 20 m/s.

Since the AP is not graded, information is encoded in the rate of the APs, not in the amplitude. In the central nervous system, the phase of the AP with respect to a large-scale oscillatory signal also appears to convey information (for reviews, see e.g. Engel *et al.*, 2001; Varela *et al.*, 2001). The oscillatory signals investigated in Study P3 may act as such a reference signal.

2.1.2 Neural currents

The intracellular potential changes associated with PSPs at distal synapses give rise to a current flow along the dendrites towards the soma. When viewed at a distance much larger than the length of the dendrite, this flow can be modelled by a current dipole. The magnetic field due to a current dipole decays as $1/r^2$, where r is the distance from the dipole. In the cortex, the parallel arrangement of the apical dendrites of pyramidal neurons[1] enables *spatial summation* of the electromagnetic fields from nearby neurons. The characteristic time course of the postsynaptic currents is on the order of ten milliseconds, which is slow enough to allow for *temporal summation* of the contributions from nearby neurons to the net field. Owing to these two summation mechanisms, PSPs are the pri-

[1] The most abundant (70–80%) neuron type of the cortex.

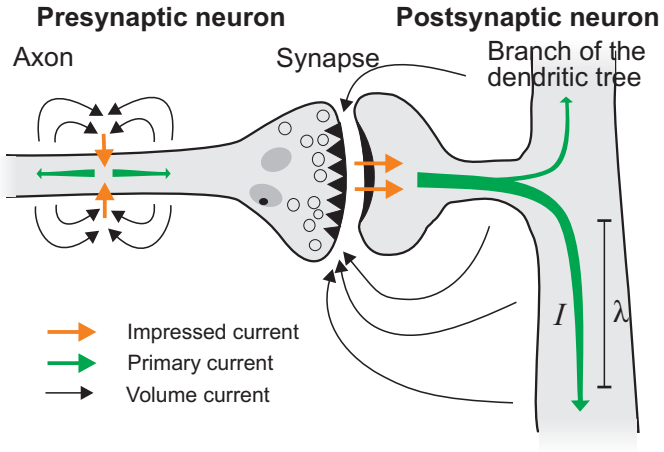

Figure 2.2 A synapse at a dendritic spine and the associated electric currents. In the presynaptic cell, the action potential gives rise to a quadrupolar source whereas in the postsynaptic cell, the currents in the dendrites are mostly dipolar. The length constant λ represents the decay of the current I due to leakage.

mary source of MEG and EEG signals.

The strength of the current dipole is defined as $Q = I\lambda$, where I is the current and λ is the *length constant* that describes the decay of the current as a function of distance. The estimates of Q of a single EPSP in the apical dendrite of a pyramidal cell depend on the assumed geometry; theoretical calculations have suggested 50 fAm (Okada, 1982), 120 fAm (Vvedensky *et al.*, 1985), and 20 fAm (Hämäläinen *et al.*, 1993). A simulation study employing realistic 3D models of cortical neurons indicated considerably larger values of 290–900 fAm and a non-vanishing contribution from basal dendrites (Murakami and Okada, 2006).

For an action potential, the situation is quite different; the intracellular currents flow almost symmetrically both forward and backward from the location of the AP peak[2]. Such a current constellation forms a quadrupole, and the associated magnetic field decays as $1/r^3$, that is, much faster than the field of a current dipole. This rapid attenuation of the field as a function of distance and the less likely temporal summation due to the short duration of the APs render them almost invisible in MEG and EEG. However, we recorded also axonal MEG responses in study P2. There, the *compound action potential* (CAP), formed by temporally aligned APs in several parallel nerve fibres in the nerve trunk, is a

[2]For example, for an AP duration of 1 ms, the forward and backward fronts are separated by 20 mm in an axon with a conduction velocity of 20 m/s.

result of an analogous summation as in the case of PSPs. Still, the symmetry giving rise to the quadrupolar arrangement needs to be broken for a measurable contribution from a CAP. Such symmetry breaks arise when the nerve bends and the forward and backward currents no longer flow along the same line, and the CAP thus generates a dipolar net current distribution. Peripheral nerves have also been shown to generate detectable magnetic fields (Hari *et al.*, 1989).

The intracellular currents are accompanied by passive extracellular return or *volume currents* that close the electric circuit and thus prevent the accumulation of electric charge. These ohmic currents flow in the whole surrounding conducting medium but have the highest density in the vicinity of the cells that drive them. For modelling purposes, it is convenient to define *impressed currents* as those directly associated with the influx or outflux of ions through the cell membrane, *primary currents* as those within the cell, and volume currents as the currents driven by the primary currents; the respective current densities are usually denoted as $\mathbf{J}_\mathrm{i}(\mathbf{r})$, $\mathbf{J}_\mathrm{p}(\mathbf{r})$ and $\mathbf{J}_\mathrm{v}(\mathbf{r})$. This division is illustrated in Fig. 2.2. The impressed currents, while being the driving force, flow for such a short distance that their dipole moment Q is very small compared with that of the other currents, and thus their direct effect on the extracranial electromagnetic fields can be neglected (Tripp, 1981).

2.2 Instrumentation for magnetoencephalography

2.2.1 Signal strength

Extracranial neuromagnetic fields are extremely weak. Figure 2.3 shows the magnetic spectrum obtained with a helmet-shaped 306-channel magnetometer array (Elekta Neuromag Oy, Helsinki, Finland), both in the absence of a subject and from a resting subject. The spectral density of the 10-Hz peak of the spontaneous brain activity is less than $100\,\mathrm{fT}/\sqrt{\mathrm{Hz}}$. Brain's physiological evoked responses (not shown in the Figure) are on the order of 100 fT in amplitude. In Study P2, the detected responses with peak amplitudes slightly less than 5 fT were among the weakest seen by MEG. Earth's steady magnetic field (50–90 μT) is thus about 10^{10} times stronger than the faintest MEG signals measured so far.

Assuming a dipole moment $Q = 500$ fAm for a single EPSP (see Sec. 2.1.2 and Murakami and Okada, 2006), a spherical volume conductor (see Sec. 2.4.1) with a radius of 8 cm,

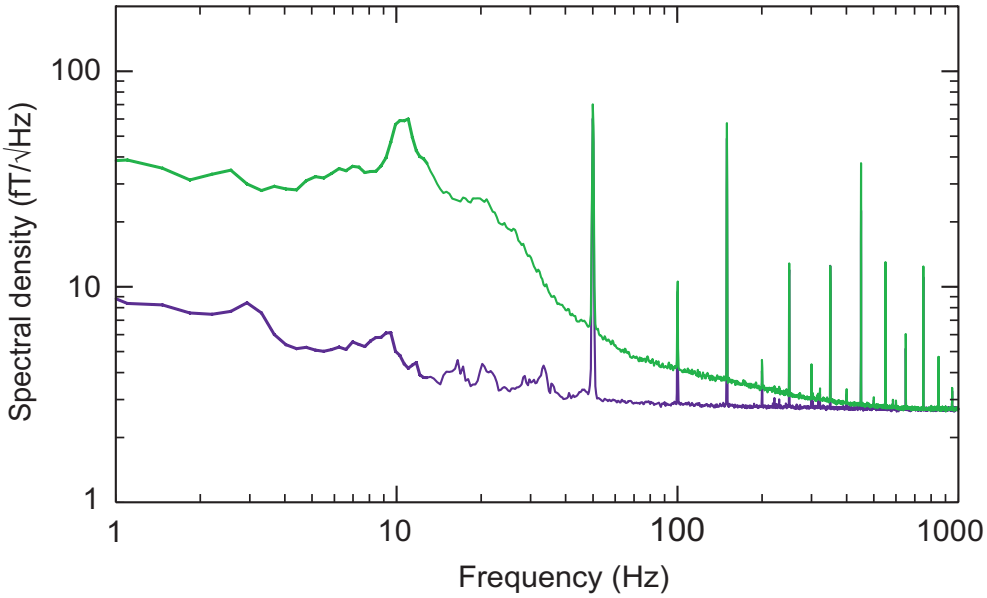

Figure 2.3 Spectral densities of magnetic fields as a function of frequency in the absence of a subject (blue) and with a subject resting (green). These spectra are the average of the spectra of all 102 magnetometer signals recorded with the Elekta Neuromag whole-scalp neuromagnetometer. *Author's unpublished data*.

and a perfectly parallel and tangential orientation of the contributing dendrites 2 cm below the surface of the sphere, the magnetic field 2 cm above the surface would exceed 100 fT only when more than 10,000 perfectly simultaneous EPSPs take place. In reality, the orientations of the dendrites and their branches are less optimal for MEG, and the EPSPs do not fully overlap temporally. Therefore, it can be estimated that tens of thousands of active neurons are required for generation of fields on the order of 100 fT.

Local synchrony of the PSPs affects the field strength. As a first approximation, tightly stimulus-locked postsynaptic activity sums up linearly, whereas N neurons with randomly-timed PSPs summate only in proportion to $\sqrt{N}$. It can be shown that synchronising 1% of the elements (neurons) in a population of 10^5 elements yields already 80% of the maximum signal that the population of can generate; in larger populations, the percentage is even higher (Hari, 1990).

The challenge of MEG is to detect the weak fields but also to suppress the ambient, disturbing magnetic fields that are several orders of magnitude stronger. A combination of several techniques is required to achieve these goals.

2.2.2 Sensors and systems

Magnetic signals due to the activity of the human brain were first detected by a conventional induction magnetometer but with a very low signal-to-noise ratio (Cohen, 1968). The advent of the SQUID (superconducting quantum interference device) sensor with its exceptional sensitivity (Zimmerman *et al.*, 1970) enabled practical MEG measurements (Cohen, 1972). Since then, MEG sensors and devices have evolved to reach lower noise levels and larger coverage. An important milestone was the introduction of the first whole-scalp device (Ahonen *et al.*, 1993b).

A SQUID is a superconducting loop interrupted by one or two *Josephson junctions* (Josephson, 1962), which is a thin ($\approx$ 100 nm) layer of an electric insulator between two superconductors. The electron pairs of the superconductor can tunnel through the junctions, giving rise to an interference that manifests itself as a dynamic resistance that depends on the magnetic flux applied through the SQUID loop. This dependence is non-linear and periodic, and therefore SQUIDs are operated in a negative feedback loop known as a *flux-locked loop*. In this mode, the SQUID acts as a zero flux detector; a feedback coil is attached on top of the SQUID loop and a controller adjusts the feedback current so that the SQUID output remains zero, that is, the feedback is set to exactly cancel the measured flux. This feedback current is directly proportional to the measured flux. Due to the intrinsic periodic response, SQUIDs as such cannot measure absolute flux values and magnetic fields strengths but only their changes.

The SQUID loop is made small ($d << 1$ mm) to optimise the noise performance. Such a loop couples only weakly to the external magnetic field. To enhance this coupling and to enable measurements of various components of the magnetic field, MEG sensors employ superconducting *flux transformers* that have a large *pick-up coil* ($d \approx$ 2–3 cm) and a small but multiturn *signal coil* attached on top of the SQUID loop, connected in series. The field in the pick-up coil gives rise to a shielding current that also passes through the signal coil where it generates flux threading the SQUID loop.

The geometry of the pick-up coil determines the field component it measures. A simple loop forms a *magnetometer* that measures the field component normal to the loop surface, i.e., B_z, where z is the direction along the normal. Two oppositely-wound loops make up a *gradiometer* whose output approximates a spatial derivative of the field. If these loops are in a plane, the sensor is a planar gradiometer measuring $\partial B_z/\partial x$; if they are on the same axis, it is an axial gradiometer that measures $\partial B_z/\partial z$. Figure 2.4 shows the three

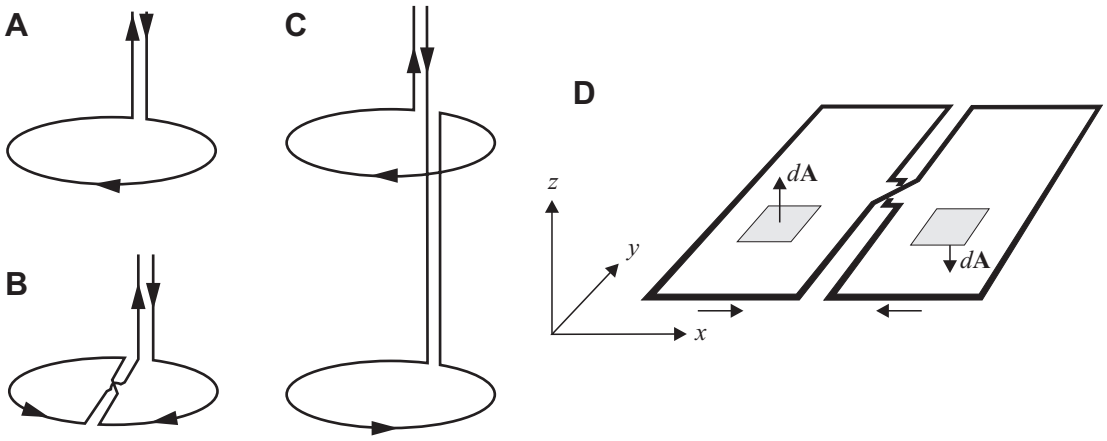

Figure 2.4 Common pick-up coil geometries: **A** magnetometer, **B** planar gradiometer, and **C** axial gradiometer. **D** The output of a sensor is computed as a surface integral with an integration element $d\mathbf{A}$ normal to the coil. *Adapted from Hämäläinen* et al. *(1993).*

most common types of pick-up coils.

The output of the i'th channel is

$$b_i = \int_S \mathbf{B}(\mathbf{r}) \cdot d\mathbf{A} \approx \sum_{k=1}^{K} w_k \mathbf{B}(\mathbf{r}) \cdot \mathbf{n}_k \tag{2.1}$$

where S is the surface of the pick-up coil; see Fig. 2.4D. The output is approximated by computing the field $\mathbf{B}(\mathbf{r})$ at K discrete points (see Sec. 2.4.1), projecting the field onto the normal vector $\mathbf{n}_k$, and weighting by w_k.

The field component measured by the sensor determines its sensitivity to a particular current distribution. This sensitivity pattern can be expressed as a *lead field*, which is a fictitious vector field that gives the output of a channel to a unit dipolar source current at a given location and orientation. Figure 2.5 illustrates the lead fields of the previous three pick-up coil geometries. A magnetometer or an axial gradiometer outputs the largest signal for source currents around the pick-up coil and no signal for a source current at or beneath the centre of the coil, whereas planar gradiometers give the maximum signal for source currents directly beneath them. It can be shown that the lead fields of orthogonal planar gradiometers and a magnetometer at the same location and plane are orthogonal, and thus the three sensors provide independent information about the sources (Ahonen *et al.*, 1993a).

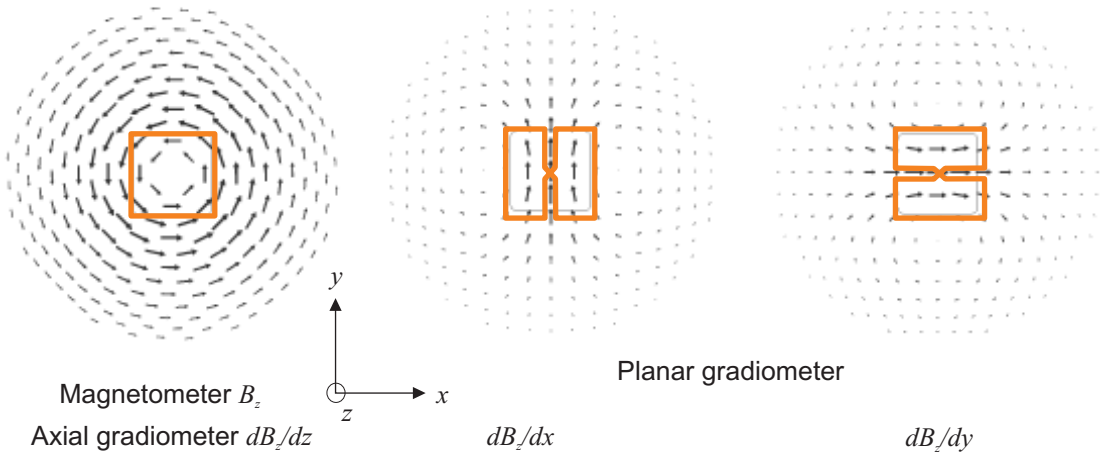

Figure 2.5 Lead fields associated with common pick-up coil geometries.

The data for the studies comprising this Thesis have been acquired with a 306-channel MEG device (Elekta Neuromag Oy, formerly Neuromag Oy, Helsinki, Finland) which employs 102 triple-sensor elements in a helmet-shaped array. Each sensor element comprises a magnetometer measuring B_z and a pair of orthogonal planar gradiometers measuring $\partial B_z/\partial x$ and $\partial B_z/\partial y$. The complementarity of the two types of sensors was also exploited: in Study P2, we employed exclusively the magnetometers as their lead fields reach deep brain structures better than those of the gradiometer sensors, whereas in Study P3 the focality of the planar gradiometers allowed investigating phase locking between two cortical areas at the sensor level. In P1 and P5, data from the whole sensor array were utilised, and in P4 the source modelling was guided with the planar gradiometer signals but eventually both sensor types were used.

2.2.3 Interference suppression

The weakness of cerebral magnetic fields necessitates effective means to block the ambient interference, often several orders of magnitude stronger. Multiple methods are usually employed in parallel: *i*) the MEG system is operated in a magnetically shielded room, *ii*) gradiometer sensors are utilised for their low sensitivity to far-away sources whose fields are nearly homogeneous, and *iii*) any residual interference is estimated and removed from the data computationally. These techniques and their commonly used variants are briefly explained below.

Magnetically shielded rooms rely on high permeability *mu-metal* (an alloy of nickel and iron) which reduces the field strength within the room by providing the external fields a low reluctance path along the walls of the room. At frequencies above some tens of hertz, the shielding relies on eddy currents that flow in a layer of high-conductivity material, usually aluminium, counteracting the impinging fields. For efficient shielding across a range of frequencies, the walls are typically made of a combination of mu-metal and aluminium plates (Kelhä *et al.*, 1982). Shielded rooms usually employ 2 or 3 such shells, or layers, to increase the shielding factor, particularly at frequencies below 10 Hz.

Passive magnetic shields can be enhanced by active systems that measure the interference field and generate a compensating field to cancel the interference at the location of the MEG system. A typical *active compensation system* comprises a flux-gate sensor, driver electronics, and pairs of Helmholtz coils outside of the room to supply the cancellation fields. Such a setup can provide 10–30 dB of additional shielding if the interference sources are far away (tens of meters or more) so that the interferring fields are approximately homogeneous at the location of the room. Unfortunately, nearby sources may be problematic since proper compensation would require the spatial derivatives of the field to be taken into account. Recently, single-shell light-weight shielded rooms, supported by active compensation systems also inside the shielded room, have been successfully utilised with MEG (for a performance verification, see De Tiège *et al.*, 2008). The data for the studies in this Thesis were acquired in a two-layer room (ETS Lindgren Oy, Eura, Finland) equipped with an external active compensation system.

Employing gradiometers instead of magnetometers is a straightforward method to protect the MEG sensors from far-away interference sources; the response of a gradiometer to a source falls off much faster with distance than that of a magnetometer. A carefully manufactured (well-balanced) gradiometer can attenuate homogeneous fields by as much as 60 dB (factor of 1,000). On the other hand, Study P2 demonstrates that fields from the most distant brain regions are picked up better by magnetometers than gradiometers.

Interference can also be measured explicitly and then subtracted from the signals. *Reference sensors* located some tens of centimetres away from the MEG helmet do not measure brain signals but capture mainly the interference. By optimally coupling the output of the reference sensor array to the MEG channels proper, the interfering signal can be removed. This arrangement works well with homogeneous interference fields; however, the presence of gradients may degrade the performance as the interference at the helmet must be extrapolated from the measurements at the reference sensors. For this purpose, the refer-

ence sensor arrays usually include both magnetometers and gradiometers. The reference sensor approach can also be considered as a way to construct higher-order gradiometers (Vrba and Robinson, 2001).

Interference can be suppressed without a reference sensor array since external interference and brain sources evoke different spatial patterns on the sensor helmet. The benefit of this reference-free approach is that no extrapolation is required since the interference is measured at the very location it should be suppressed. The approach relies on the concept of *signal space* which is a virtual space where each measurement channel spans one dimension. Thus, the output of an n-channel sensor array at any time instant can be expressed as a *signal vector* in the n-dimensional signal space. The spatial pattern is equal to the direction of the corresponding vector in the signal space while the overall strength of the signal defines the length of that vector. If the subspace where the interference resides is known, the measured signals can be projected onto a hyperplane orthogonal to that subspace, thus completely removing the contribution of the unwanted subspace; the method is called *signal-space projection* (SSP) (Tesche *et al.*, 1995; Uusitalo and Ilmoniemi, 1997; Parkkonen *et al.*, 1999).

Projected data are rank deficient, i.e., after projecting out an m-dimensional subspace from an n-channel measurement, only $n - m$ linearly independent signals are left. Since m is usually only 3–8 and $n > 100$, the mere loss of degrees of freedom is not a problem as such, but to correctly interpret the spatial aspect of the projected data, the effect of the SSP operator should be taken into account because SSP may introduce slight changes in the signal topography. In source modelling, the projection operator has to be applied to the result of the forward computation to ensure unbiased estimation.

The interference subspace is usually determined by principal component analysis (PCA) of a short measurement without a subject. Selecting 3–5 components associated with the highest eigenvalues for the subspace typically reduces the variance of the interference down to acceptable levels. Such subspaces appear very stable over time, even for months or years, provided that the magnetic environment does not change drastically.

The interference subspace can be optimised to the frequency band of interest by filtering the raw data to that band prior to PCA. The magnetic auditory brainstem responses (mABR) measured in Study P2 were concentrated at frequencies above 200 Hz. Applying PCA on the band-pass filtered (180–1000 Hz) data yielded only two significant components, corresponding to the harmonics of the mains, instead of the typical five that include

components for homogeneous fields. Suppressing homogeneous fields would have attenuated the spatially smooth brainstem signals considerably.

Instead of determining the interference subspace statistically, the known physical properties of magnetic fields—expressed in Maxwell's equations—can be utilised to mathematically delimit the subspace where all signals due to sources external to the sensor helmet must reside. Similarly, another subspace can be spanned for all signals whose sources are inside the sensor helmet. These two subspaces are linearly independent, thus providing a unique way of separating the measured data into contributions from outside and inside of the sensor helmet. Interference suppression can now be performed simply by dropping out the outside contribution. This method is called *signal-space separation* (SSS) (Taulu and Kajola, 2005).

The SSS subspaces are derived from a series of spherical harmonic functions. In the SSS framework, the data are first expressed as two multipole expansions, one for the inside and the other for the outside contribution, in spherical harmonic spaces. Subsequently, the sensor-level data are reconstructed using only the inside expansion. Both series are truncated to stay within the limits imposed by the number of channels in the system; the inside expansion typically corresponds to about 100 degrees of freedom. The SSS method is thus data-independent and time-invariant; however, it does require precise information on the geometry of the sensor array. SSS was employed in Studies P1 and P5.

2.3 Signal processing

2.3.1 Averaging and filtering

MEG signals related to a single stimulus presentation or task performance usually have too low a SNR for reliable detection and modelling of brain activity. Therefore, signals to multiple such events are typically averaged to suppress the uncorrelated noise present in the recording, yielding an *average response*. In averaging, the stimulus- or task-locked signal components are retained and the uncorrelated components decrease at best as $1/\sqrt{N}$, where N is the number of trials. However, the responses may also change in the course of multiple trials due to, e.g., habituation, loss of attention, and decreasing vigilance. The earliest responses are typically the least susceptible to this kind of variation (Hari, 1990), and the experimental design can be optimised for a given response (Ahlfors *et al.*, 1993). In Study P2, we presented about $16,000$ stimuli in 30 minutes and averaged

the brainstem responses without an appreciable suppression of the response with respect to a slower stimulation rate. On the other hand, less than 100 trials were sufficient in P3, P4, and in the experimental part of P1. Single-trial responses can be studied as well (see e.g. Tanskanen *et al.*, 2007).

The noise uncorrelated to the stimulus presentation is not only due to background brain activity and other physiological sources, such as muscular activity, but it also results from the instrumentation and environment. The relative contributions of these factors depend on the frequency. At low frequencies (< 1 Hz), the environmental and non-neural physiological sources can be difficult to suppress and thus may contaminate the recordings. In addition, the $1/f$ noise of the SQUID sensors elevate the system noise at these frequencies. The predominant brain rhythms span frequencies from a few to some tens of Hz; within this band, the background brain activity plays the major role. For higher frequencies, the intrinsic system noise gives the largest contribution provided that no strong muscular activity takes place; see Fig. 2.3. The exceptional high-frequency responses investigated in P2 are within this high-frequency band and would have thus benefited from a lower system noise level. The experimental data in the other studies concentrated on frequencies less than 100 Hz.

To improve the SNR of a particular response, the MEG data are filtered temporally and spatially. Temporal filtering includes typical time-domain band-pass filtering but also, e.g., template matching to detect single responses. Spatial filtering can be as simple as selecting and examining the signal of a MEG channel above the source area but can also involve source modelling or beamforming (see Sec. 2.4), or blind source separation techniques such as *independent component analysis* (ICA) (for a review, see Hyvärinen and Oja, 2000).

2.3.2 Extracting oscillatory responses from MEG data

The stimulus-locked time-domain averaging described earlier is not applicable for recovering the amplitudes of oscillatory brain signals as the phase of these signals is typically not locked to the stimulus. Instead, the phase information has to be removed so that averaging is guaranteed to improve the signal-to-noise ratio. Alternatively, the phase itself can be investigated, as in Study P3.

Several methods exist for estimating the amplitudes of the oscillatory signals. The choice

depends on the required temporal granularity at which one needs to follow the spectral content of the measurements. In certain cases, the data can be considered stationary, i.e., the frequency composition is assumed not to vary over time, whereas in other cases the non-stationarity is at the focus of interest.

Fourier transform

The spectrum of a long span of data, e.g., a task block of several tens of seconds or the entire experiment, is typically computed using the *Welch method*: the magnitudes of the fast Fourier transforms (FFTs) of half-overlapping segments of the data are averaged. Prior to FFT, a temporal window function is applied to each segment to optimise the resolution of the transform. This piecewise approach enables the use of FFT and thus presents a significant computational advantage over the plain Fourier transform (FT) applied to the entire data at once. Averaging reduces the variation of the spectral estimate but it also implies poorer frequency resolution due to the shorter length of the transform. In P5, we employed the Welch method with 4096-sample-long Hanning-windowed FFTs to estimate the amplitude spectra with a frequency resolution of 0.073 Hz; see Fig. 2.

Slow changes in the spectral content of a signal can be monitored by computing the FFTs as above but omitting the averaging step. This approach, referred to as short-time Fourier transform (STFT), yields coarse time series of the frequency components across the data. For the frequencies in typical MEG signals, the length of the segment, i.e., the support of the transform, has to be 1 s or longer for a reasonable frequency resolution. This limited temporal resolution is sufficient, e.g., for quantifying spectral differences between two or more alternating experimental conditions, or for tracking spontaneous changes in rhythmic activity; however, it does not allow quantifying the sub-second modulations of spontaneous brain rhythms by external stimuli, for example.

Modelling

The STFT may not be optimal for analysing narrow-band signals; the frequency bins (the discrete set of frequencies at the output) are determined solely by the support of the FFT, and it may thus happen that no bin is centred at the desired frequency. In addition, within the finite support of the STFT, most frequency pairs are non-orthogonal and spectral leakage compromises amplitude and phase estimation. If the data contain a known sparse set of signals at distinct frequencies, the STFT can be replaced by a *general linear model*

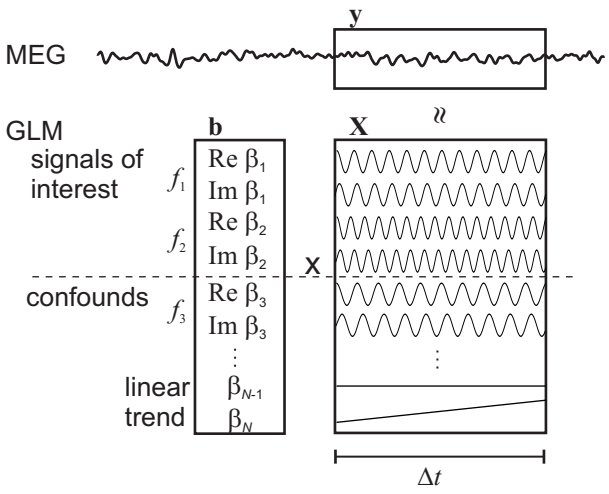

Figure 2.6 Obtaining the amplitudes of a small set of frequencies (f_1 and f_2) using a general linear model (GLM). *Adapted from P5.*

(GLM) with model sinusoids as regressors in the design matrix. If the phases of those signals are not known, quadratures should be included. The quadrature component of an arbitrary regressor can be obtained by a Hilbert transform; for a sine wave it is simply the cosine wave, i.e., a 90-degree-shifted copy. Applying Euler's formula $e^{ia} = \cos a + i \sin a$, the complex-valued model can be written as

$$\mathbf{x}(t) = \begin{pmatrix} e^{i2\pi f_1 t} \\ e^{i2\pi f_2 t} \\ \cdots \\ e^{i2\pi f_N t} \\ t \\ 1 \end{pmatrix} \tag{2.2}$$

where the two lowest rows correspond to a linear trend. Instead of using complex-valued regressors, the sinusoidal quadratures can be included as separate sin and cos terms. The design matrix can then be constructed for an arbitrary time interval of M samples as

$$\mathbf{X} = (\mathbf{x}(t_1)\, \mathbf{x}(t_2)\, \cdots\, \mathbf{x}(t_M)) \tag{2.3}$$

where the $\mathbf{x}(t)$'s are column vectors. This matrix is the transpose of the usual GLM design matrix so that each row holds a time series. Figure 2.6 illustrates a design matrix that contains four regressors of interest, corresponding to the quadratures of two sinusoids

at frequencies f_1 and f_2, and additional "nuisance regressors" that model the known but uninteresting non-white components of the data. The inclusion of such regressors aims to cancel the spurious effects of these interferring signals on the estimates of the signals of interest. The time-dependent MEG data, represented as a row vector $\mathbf{y}$ for each channel, can be modelled as

$$\mathbf{y} = \mathbf{bX} + \mathbf{e} \tag{2.4}$$

where $\mathbf{b}$ is a row vector of the unknown complex amplitude coefficients β_n. The error term $\mathbf{e}$ is assumed to be normally distributed. Provided that $\mathbf{X}$ is full rank (the regressors are linearly independent), the solution that minimises $\mathbf{e}$ in the least-squares sense is

$$\hat{\mathbf{b}} = \mathbf{y}(\mathbf{X}^{\mathrm{T}}\mathbf{X})^{-1}\mathbf{X}^{\mathrm{T}} = \mathbf{y}\mathbf{X}^{+} \tag{2.5}$$

where $^{+}$ denotes the pseudo-inversion of a matrix. The amplitudes a_n and phases ϕ_n of the regressors are then obtained as

$$a_n = 2\|\beta_n\| \tag{2.6}$$

$$\phi_n = \angle\,\beta_n \tag{2.7}$$

where the $\angle$ operator refers to taking the phase angle of a complex number.

In P5, we applied this GLM-based method to estimate the amplitudes of oscillatory signals evoked by a frequency-tagged stimulus. The analysis was done for 1-s windows temporally aligned with the experimental conditions. STFT would not have enabled sufficient accuracy in the estimation of the tag-related signal amplitudes.

Wavelets

For a more balanced trade-off between temporal and frequency resolution, *wavelets* can be employed to quantify the instantaneous amplitude and phase of a continuous signal. Wavelets are oscillatory functions of finite length and they can be scaled and translated to match signal components at specific frequencies and time points, respectively. The idea of such analysis for non-stationary data was conceived by Gabor (1946) but the proper mathematical foundations of the *wavelet transform* were laid later (Morlet *et al.*, 1982; Daubechies, 1988). A wavelet transform is a way to perform *multiresolution analysis*: lower frequencies are localised in time with less precision than higher frequencies and, conversely, lower frequencies are localised in frequency with higher precision than higher

frequencies. The resolution of the wavelet transform, just as that of a FT, is limited by the *uncertainty principle*, which imposes a lower bound on the product of the temporal resolution (Δt) and frequency resolution (Δf).

The wavelet transform can be performed by convolving the time domain signal with scaled versions of the prototype or *mother wavelet*. Owing to the lower temporal accuracy at lower frequencies, the corresponding convolutions can be presented at lower sampling rates; however, this frequency-dependent sampling is usually undesirable in MEG/EEG analysis. Instead, the convolution result is used as is, such as in a Gabor filter (Sinkkonen *et al.*, 1995; Tallon-Baudry *et al.*, 1997).

In studies P3 and P5, we employed a Morlet (1982) wavelet, in which the oscillatory component is a complex sinusoid at a single frequency, and its temporal localisation is obtained by shaping the envelope with a Gaussian:

$$w(t,t_0,f_0) = C \cdot e^{-\frac{(t-t_0)^2}{2\sigma_t^2}} \cdot e^{i2\pi f_0(t-t_0)} \tag{2.8}$$

$$\sigma_f = \frac{f_0}{\lambda} \tag{2.9}$$

$$\sigma_t = \frac{\lambda}{2\pi f_0} \tag{2.10}$$

$$C = \frac{1}{\sqrt{\sigma_t \sqrt{\pi}}} \tag{2.11}$$

where t is time, t_0 and f_0 are the centre time and frequency, respectively, and the length parameter λ controls the trade-off between the frequency and time resolution. The variables σ_t and σ_f are the standard deviations of the wavelet in the time and frequency domain, respectively. The normalisation term C ensures that $\int_{-\infty}^{\infty} |w(t,t_0,f_0)|^2 dt = 1$, i.e., the wavelet is normalised for unit energy. The real and imaginary parts, corresponding to the cosine and sine terms, are shown in Fig. 2.7. These wavelets do not have compact support and, for any finite interval, they do not form an orthogonal basis. The Daubechies (1988) wavelets have these desirable properties but their interpretation is not as intuitive as that of Morlet wavelets, which can directly be associated with pure sinusoids.

Convolution of a real-valued continuous signal $s(t)$ with a Morlet wavelet yields a complex signal whose modulus and angle give the instantaneous amplitude $a(t)$ and phase

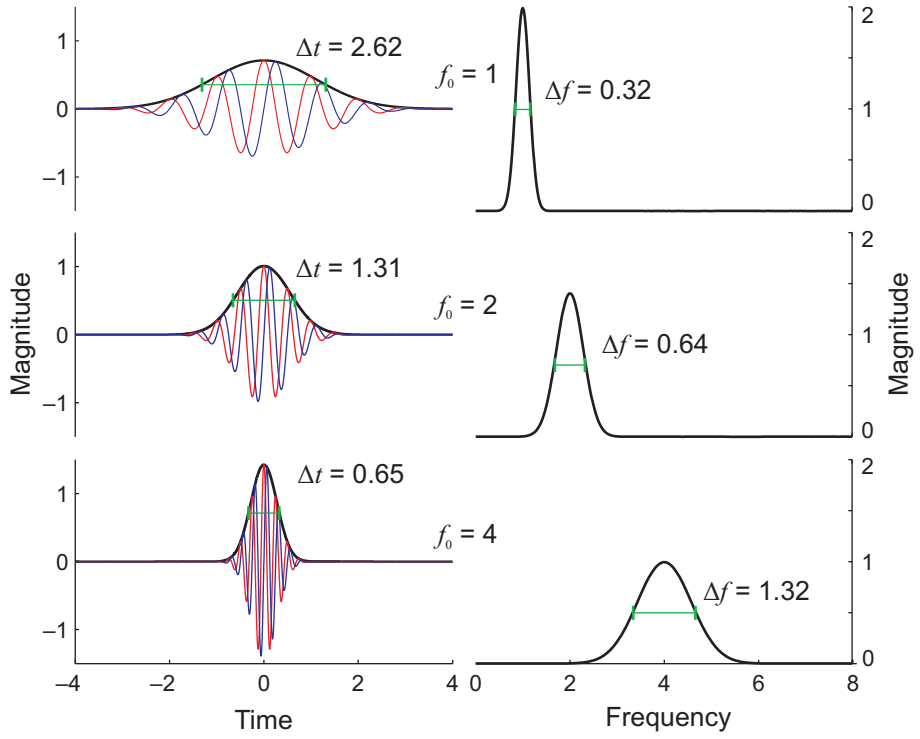

Figure 2.7 Morlet wavelets ($\lambda = 7$) scaled for frequencies $f_0 = 1$, 2 and 4 (arbitrary units). The time-domain plots (left column) show the magnitude (black), as well as the real (red) and imaginary (blue) components. With an increasing frequency, the wavelets shrink in time (left column) and dilate in frequency (right column). Δt and Δf (green) indicate the full width at half-maximum (FWHM).

$\phi(t)$, respectively, at the frequency f of the wavelet:

$$a(t,f) = \|w(t,0,f) * s(t)\| \tag{2.12}$$

$$\phi(t,f) = \angle\, w(t,0,f) * s(t) \tag{2.13}$$

where $*$ denotes convolution. This decomposition directly lends itself to a *time–frequency representation* (TFR) of the signal; by plotting $a(t,f)$ or $\phi(t,f)$ so that time and frequency are along orthogonal axes, one can visualise the time- and frequency-dependent amplitude and phase of the signal. Averaging $a(t,f)$ or $|a(t,f)|^2$ across trials yields an average TFR that reflects both the stimulus-locked and stimulus-induced, i.e. non-phase-locked, activity in response to a stimulus. Studies P3 and P5 include such plots.

2.3.3 Phase-locking analysis

Information can be conveyed in the amplitude of a signal but also in its phase. Two signals that maintain a constant phase difference are said to be phase-locked with each other. In electrophysiology, such phase relations can be considered as signatures of information transfer between brain areas or between the peripheral and central nervous systems. However, phase-locking of the signals from, say, two brain regions does not necessarily imply that these two regions are directly connected with each other or that they exchange information. Phase locking can also occur as a result of an external influence, such as a common signal from another brain region. On the other hand, a reproducible coincidental phase locking is improbable: locking does imply that the involved areas share some information, and therefore it is worthwhile to study the phase relations between brain signals.

The methods described in the previous section yield an estimate of both amplitude and phase. The obtained phase information can be subjected to phase-locking analysis. As in the amplitude analysis, there is a tradeoff between frequency and temporal resolutions. While STFT can be used to study phase relationships, the instantaneous phase provided by wavelets opens up new domains for such analysis. The following paragraphs concentrate on the subsequent analysis of these continuous estimates of phases.

Averaging $\phi_n(t,f)$ across trials n in an MEG experiment yields an estimate where high values indicate consistent phase information in the brain responses whereas low values indicate randomness. This quantity, known as the *phase-locking factor* (PLF) (Tallon-Baudry *et al.*, 1996), is typically illustrated as a time–frequency plot. PLF is closely related to the frequency content of the time-domain average described in Sec. 2.3.1, since both approaches preserve only the components whose phase is locked to the trial.

PLF can be extended to study the consistency of the phase difference between two signals $s_1(t)$ and $s_2(t)$. The *Phase-locking value* (PLV) (Lachaux *et al.*, 1999) is computed by averaging the complex phase differences

$$\Theta_n(t,f) = e^{i\delta_n} \text{ , where} \tag{2.14}$$

$$\delta_n = \phi_{1,n}(t,f) - \phi_{2,n}(t,f) \tag{2.15}$$

for each time and frequency across the trials n, *viz.*

$$P(t,f) = \frac{1}{N}\sum_{n=1}^{N}\Theta_n(t,f). \tag{2.16}$$

Now, $\angle P(t,f)$ gives the average phase difference at frequency f between these two signals for each time point t in the trial, and $\|P(t,f)\| \leq 1$ indicates the consistency of that difference; if the same difference is maintained during all trials, $\|P(t,f)\| = 1$, and if the difference varies randomly, that function will tend to zero. Importantly, $P(t,f)$ does not depend on the absolute phase of the signals with respect to the trial timing. PLV is thus able to capture *induced phase locking*.

When studying the phase locking of ongoing rhythmic MEG signals, evoked responses may present a spurious contribution to the phase information if their frequency content overlaps with the band within which phase locking is assessed. Such effects can be removed by thresholding the PLV estimate with respect to a *surrogate data set*, generated by multiple random permutations of the N trials of $\phi_{2,n}(t,f)$ in Eq. (2.15). The permutation preserves only such evoked phase locking in which the absolute phase remains constant, and suppresses induced phase locking. The surrogate data thus provide a reference condition that represents phase locking in other than induced activity and determine a threshold for the PLV to create a *phase-locking statistic* (PLS) of the data (Lachaux *et al.*, 1999). We employed this approach in P3 to account for the effect of the somatosensory evoked responses when studying the induced phase locking at around 20 Hz between the primary (SI) and secondary (SII) somatosensory cortices.

2.4 Source modelling

MEG measurements convey temporal and spatial information about neural activity. While both aspects are present in the sensor level signals, the picture of the underlying activity can be considerably refined by applying modelling techniques that enable localisation of the sources of the activity. Spatial localisation often allows better separation of the temporal behaviour of simultaneously active sources. However, the source localisation problem is a difficult one; the underlying source constellation cannot be uniquely determined from MEG/EEG data, therefore constraining models have to be employed.

The goal in source modelling is to estimate the source constellation that generates signals

that best match the measured MEG. This endeavour entails two distinct tasks: *i)* given a source constellation, predicting what the measurements (observed magnetic or electric fields) would be, and *ii)* given the measurements, estimating the source constellation such that the prediction best matches the measurements. A solution to the former part, the *forward problem*, is required to tackle the second part, the *inverse problem*. Both problems involve their specific models, and the range of these models has lead to families of source modelling algorithms. The following sections review the approaches and models applied in this Thesis.

2.4.1 From neural currents to magnetic fields

Magnetic field $\mathbf{B}$ external to the brain, elicited by a known primary current distribution $\mathbf{J}_\mathrm{p}$ (see Sec. 2.1.2), can be computed uniquely. In principle, the accuracy of the result depends only on the accuracy of the geometry and conductivity information about the structures where the volume currents $\mathbf{J}_\mathrm{v}$ flow. Since all currents contribute to the external magnetic field, the computations must consider the total current density $\mathbf{J}$. The following mathematical treatment mostly follows that by Sarvas (1987), with additional details from the reviews by Hämäläinen *et al.* (1993) and Baillet *et al.* (2001).

Field computations

Electric and magnetic fields are governed by *Maxwell's equations*. Since the neural currents and fields vary slowly ($f \lesssim 1$ kHz) in a small volume, the time-dependent terms can be neglected and the *quasistatic approximation* (Plonsey, 1969; Hämäläinen *et al.*, 1993) can be applied such that

$$\nabla \cdot \mathbf{E} = \frac{\rho}{\varepsilon_0} \tag{2.17}$$

$$\nabla \cdot \mathbf{B} = 0 \tag{2.18}$$

$$\nabla \times \mathbf{E} = -\frac{\partial \mathbf{B}}{\partial t} \approx 0 \tag{2.19}$$

$$\nabla \times \mathbf{B} = \mu_o \mathbf{J} + \mu_0 \varepsilon_0 \frac{\partial \mathbf{E}}{\partial t} \approx \mu_0 \mathbf{J} \tag{2.20}$$

where $\mathbf{E}$ is the electric field, μ_0 and ε_0 are the permeability and permittivity of free space, respectively, and ρ is the charge density. Since it is assumed that $\nabla \times \mathbf{E} = 0$, the electric field can be expressed in terms of its scalar potential V as $\mathbf{E} = -\nabla V$. Volume currents are

driven by the electric field $\mathbf{E}$ according to Ohm's law. Thus, the total current density

$$\mathbf{J} = \mathbf{J}_\mathrm{p} + \mathbf{J}_\mathrm{v} = \mathbf{J}_\mathrm{p} + \sigma\mathbf{E} = \mathbf{J}_\mathrm{p} - \sigma\nabla V \tag{2.21}$$

where σ is the conductivity of the medium. From Eq. (2.20) and the vector identity $\nabla \cdot \nabla \times \mathbf{A} = 0$, it follows that $\nabla \cdot \mathbf{J} = 0$. Thus, Eq. (2.21) can be written as $\nabla \cdot (\sigma\nabla V) = \nabla \cdot \mathbf{J}_\mathrm{p}$, which yields (assuming constant σ)

$$\Delta V = \frac{1}{\sigma}\nabla \cdot \mathbf{J}_\mathrm{p} \tag{2.22}$$

where Δ denotes the Laplace operator. This equation connects the electric potential—and thus the volume current distribution—to the primary current distribution. In general, the solution can only be obtained numerically; however, analytic solutions exist for certain symmetries, particularly for spherical symmetry. Once the total current is known, the Biot–Savart law as a solution to Eq. (2.20) gives the magnetic field as

$$\mathbf{B}(\mathbf{r}) = \frac{\mu_0}{4\pi}\int_G \mathbf{J}(\mathbf{r}') \times \frac{\mathbf{r} - \mathbf{r}'}{\|\mathbf{r} - \mathbf{r}'\|^3} dv' \tag{2.23}$$

where G is the volume in which the currents flow.

Current dipole

An elementary current is a useful concept when computing the external magnetic field. It is evident from the previous equations that the field depends linearly on the magnitude of the current. Thus, any primary current distribution can be decomposed in terms of these elementary currents, and the associated magnetic field can be computed by superposition, i.e., by summing the elementary contributions. A *current dipole* is such a concept. It is a point-like concentration of current and comprises, in mathematical terms, a current source and sink an infinitesimal distance apart. A current dipole is characterised by position $\mathbf{r}'$ and moment $\mathbf{Q}$, which incorporates the orientation and strength of the current. The primary current distribution by one current dipole is thus

$$\mathbf{J}_\mathrm{p}(\mathbf{r}) = \mathbf{Q}\delta(\mathbf{r} - \mathbf{r}') \tag{2.24}$$

where $\delta(\mathbf{r})$ is the Dirac delta function. In the following derivations, to maintain generality, an unspecific primary current distribution is considered first, followed by solutions to a dipolar $\mathbf{J}_\mathrm{p}$.

Inhomogeneous conductor

To tackle the volume current distribution and hence the fields due to it, the following simplifying assumptions are useful: the conductivity outside the volume G is zero, and G can be divided into N compartments G_i within which the conductivity is constant and has the value σ_i. Now, substituting Eq. (2.21) into (2.23) yields

$$\mathbf{B}(\mathbf{r}) = \underbrace{\frac{\mu_0}{4\pi}\int_G \mathbf{J}_\mathrm{p}(\mathbf{r}') \times \frac{\mathbf{r}-\mathbf{r}'}{\|\mathbf{r}-\mathbf{r}'\|^3} dv'}_{\mathbf{B}_0(\mathbf{r})} - \frac{\mu_0}{4\pi}\sum_{i=1}^{N}\sigma_i \int_{G_i} \nabla V(\mathbf{r}') \times \frac{\mathbf{r}-\mathbf{r}'}{\|\mathbf{r}-\mathbf{r}'\|^3} dv' \qquad (2.25)$$

where $\mathbf{B}_0(\mathbf{r})$ is the contribution of the primary currents only, and the second term is due to the volume currents. With some vector algebra (for details, see Sarvas, 1987), the *Geselowitz formula* (Geselowitz, 1970) is obtained:

$$\mathbf{B}(\mathbf{r}) = \mathbf{B}_0(\mathbf{r}) - \frac{\mu_0}{4\pi}\sum_{i=1}^{N}(\sigma_{i,\mathrm{in}} - \sigma_{i,\mathrm{out}}) \int_{S_i} V(\mathbf{r}') \frac{\mathbf{r}-\mathbf{r}'}{\|\mathbf{r}-\mathbf{r}'\|^3} \times d\mathbf{S}_i \qquad (2.26)$$

where S_i is the surface bounding the compartment G_i and the integration element $d\mathbf{S}_i$ is normal to that surface; the equation holds for any $\mathbf{r}$, apart from locations on the surfaces S_i. This equation has two important properties regarding the volume current contribution: *i*) only the conductivity differences between the compartments matter, and *ii*) the potential V has to be computed only at the surfaces S_i. The form of the second term also indicates that the effect of the volume currents can be replaced by that of currents normal to the boundary between different conductivities. These fictitious currents are called *secondary currents*, and their magnitude is the product of the conductivity difference and the local electric potential. For the potential on surface S_i, a similar derivation (Sarvas, 1987) yields

$$V(\mathbf{r}) = \frac{1}{\sigma_{i,\mathrm{in}} + \sigma_{i,\mathrm{out}}}[2\sigma_N V_0(\mathbf{r}) - \frac{1}{2\pi}\sum_{k=1}^{N}(\sigma_{k,\mathrm{in}} - \sigma_{k,\mathrm{out}}) \int_{S_k} V(\mathbf{r}') \frac{\mathbf{r}-\mathbf{r}'}{\|\mathbf{r}-\mathbf{r}'\|^3} \cdot d\mathbf{S}_k] \qquad (2.27)$$

where V_0 is the potential exclusively due to the primary current distribution $\mathbf{J}_\mathrm{p}$, *viz.*

$$V_0(\mathbf{r}) = \frac{1}{4\pi\sigma_N}\int_G \mathbf{J}_\mathrm{p}(\mathbf{r}') \cdot \frac{\mathbf{r}-\mathbf{r}'}{\|\mathbf{r}-\mathbf{r}'\|^3} dv' \qquad (2.28)$$

which completes the solution to the problem of computing the external magnetic field due to a primary current distribution in a bounded, piecewise homogeneous conductor. To summarise, for a known primary current distribution $\mathbf{J}_\mathrm{p}(\mathbf{r})$, applying equations (2.28),

(2.27) and (2.26), in this order, gives the magnetic field $\mathbf{B}(\mathbf{r})$ outside such a conductor.

In the context of MEG, the volume G is taken to correspond to the head of the subject and its subdivisions G_i are determined according to the tissue types with different conductivities. The geometric shapes are usually determined from structural magnetic resonance images (MRI) of the subjects by segmenting the desired tissue types and tessellating the corresponding surfaces. In these *multi-compartment models*, the innermost volume G_1 is usually the brain, G_2 cerebrospinal fluid in the cranial space, G_3 the skull, and G_4 the scalp. This division is based on the known significant conductivity changes at the corresponding boundaries; the conductivities are approximately $\sigma_1 = 0.3$ S/m, $\sigma_2 = 1.8$ S/m, $\sigma_3 = 0.006$ S/m, and $\sigma_4 = 0.44$ S/m (compiled from Abascal *et al.*, 2008; Akhtari *et al.*, 2002; Baumann *et al.*, 1997; Latikka *et al.*, 2001). Since G_2 is usually very thin, it is often merged with G_1 in the conductor model. σ_3 exhibits the largest uncertainty; the skull bone comprises three layers of different conductivities and the relative thicknesses of the layers vary. In addition, bone tissue is poorly visible in MRIs and thus its accurate segmentation is difficult.

For modelling the magnetic fields due to primary currents in the neocortex, a multi-compartment model does not present a considerable improvement over a *single-compartment model*, or homogeneous model, which considers only the brain or cranial compartment (Hämäläinen and Sarvas, 1989). As only the conductivity differences matter (see Eqs. 2.26 and 2.27), there is no need to even specify the conductivity for such a model.

Spherical conductor

The previous equations simplify considerably when the conductor is spherically symmetric, i.e., the surfaces S_i are concentric spheres. Since the head and the cranial volume are roughly spherical, this special case is a relevant approximation in MEG and EEG. In particular, it can be shown that the radial component of the magnetic field

$$B_\mathrm{r}(\mathbf{r}) = \frac{\mu_0}{4\pi} \int_G \mathbf{J}_\mathrm{p}(\mathbf{r}') \times \frac{\mathbf{r} - \mathbf{r}'}{\|\mathbf{r} - \mathbf{r}'\|^3} \cdot \mathbf{e}_\mathrm{r} \, dv' \tag{2.29}$$

where $\mathbf{e}_\mathrm{r}$ is a unit vector oriented along the radius of the sphere. Most importantly, the radial component does not receive any contribution from the volume currents. However, the other field components are affected by the volume currents, and since no MEG device measures strictly the radial component, this equation is not directly applicable in practice. Yet, the result is important as it shows that a measurement of an approximately radial field

component outside an approximately spherical conductor is not severely distorted by the fields due to the volume currents.

If the primary current distribution is a current dipole (Eq. 2.24) located at $\mathbf{r}_\mathrm{d}$, the total magnetic field $\mathbf{B}(\mathbf{r})$ outside of a spherical conductor can be computed analytically as shown, e.g., by Sarvas (1987):

$$\mathbf{B}(\mathbf{r}) = \frac{\mu_0}{4\pi}\frac{F\mathbf{Q}\times\mathbf{r}_\mathrm{d} - (\mathbf{Q}\times\mathbf{r}_\mathrm{d}\cdot\mathbf{r})\nabla F}{F^2} \tag{2.30}$$

where

$$\begin{aligned} F &= a(ra + r^2 - \mathbf{r}_\mathrm{d}\cdot\mathbf{r}) \\ \nabla F &= (r^{-1}a^2 + a^{-1}\mathbf{a}\cdot\mathbf{r} + 2a + 2r)\mathbf{r} - (a + 2r + a^{-1}\mathbf{a}\cdot\mathbf{r})\mathbf{r}_\mathrm{d} \\ \mathbf{a} &= \mathbf{r} - \mathbf{r}_\mathrm{d} \\ a &= \|\mathbf{a}\| \\ r &= \|\mathbf{r}\| \end{aligned}$$

This relatively simple formula provides a computationally efficient way to obtain the field due to any current dipole in the spherically symmetric case. Equations (2.29) and (2.30) demonstrate that the conductivity profile of the sphere is irrelevant for MEG: a sphere with layers of different conductivities can be considered equivalent to a homogeneous sphere when computing the external magnetic field. The same is not true for electric fields, and thus the conductivities and the corresponding radii are required in the EEG forward computation.

Effects of source orientation and depth

In a spherical geometry, any current dipole can be expressed as the sum of its radial and tangential components. If the dipole is strictly radial, i.e., $Q = \|Q\|\mathbf{e}_\mathrm{r}$, it can be shown (cf. Eq. 2.30) that $\mathbf{B}(\mathbf{r})$ vanishes. Thus, the radial component does not produce any magnetic field outside of a spherically symmetric conductor. Because of the aforementioned approximate sphericity of the head and cranium, radial source currents in the brain indeed produce considerably weaker external magnetic fields than tangential sources of the same strength and depth. In other words, MEG is most sensitive to neural currents flowing tangential to the skull. As explained in Sec. 2.1, postsynaptic currents in the apical dendrites of pyramidal neurons are the main source of MEG. Since these dendrites, and

thus the currents, are oriented approximately perpendicularly to the local cortical surface, tangential sources are mainly in the sulcal cortex. However, since the true conductivity geometry is not exactly spherical, MEG is not completely blind to any orientation of the current. A simulation study demonstrated that only 2-mm wide strips at the crests of the gyri are characterised by poor resolvability, and that—in general—the depth of the source has a greater effect on its resolvability than orientation (Hillebrand and Barnes, 2002).

In a perfect sphere, the invisibility of radial primary currents translates to the invisibility of any current dipole at the centre of a sphere where all orientations can be considered radial. Therefore, it is questionable whether the deepest brain structures elicit sufficiently large magnetic signals for source localisation. In Study P2, we showed that the electric activity in the auditory brainstem generates magnetic responses strong enough for localisation of the sources. Again, the non-sphericity of the cranium, particularly that of the inferior part, was important for the detectability of these responses. In this study, we employed a three-compartment conductor model comprising brain, skull, and scalp volumes. With respect to a spherical model, the source locations differed by as much as 25 mm and their strengths varied substantially. The other studies in this Thesis involved only cortical sources and thus either a single-compartment model (P1, P5) or a sphere model (P1, P3, P4) was considered adequate.

2.4.2 From magnetic fields to neural currents

Estimating the primary current distribution from the magnetic (or electric) measurements outside of the head is an ill-posed problem; the solution is not unique and small changes in the data may lead to large differences in the estimates. To provide a solution, the primary current distribution has to be constrained to a model that is then fitted to the data using the forward solution discussed in the previous Section. Thus, inverse modelling involves at least two kinds of models: a conductor model, more generally a forward model, to solve the forward problem, and a source model to parametrise and constrain the primary current distribution $\mathbf{J}_\mathrm{p}(\mathbf{r})$. This Section deals with source models and the algorithms to estimate them from a MEG data set.

Signal space (see Sec. 2.2.3) is also a useful concept in source modelling. In the following sections, the signal vector $\mathbf{b}(t)$ represents the collection of signal values $b_1 \ldots b_N$ at all N MEG sensors at time t.

Bayesian approach

The MEG inverse problem is a good example of a problem whose solution requires some prior assumptions. Earlier, such assumptions were not considered in the probabilistic sense and they only implicitly manifested in the specific inverse modelling algorithm. However, in practice, much of the prior information—in addition to the data themselves—bears some uncertainty which cannot necessarily be expressed as constant variables but rather calls for probability distributions. Moreover, these uncertainties should be propagated to the results as comprehensively as possible so that the reliability of the results can be quantified. *Bayesian inference* provides the framework for this kind of analysis. There, prior information is incorporated in a principled manner as probability distributions, and also the estimates are given as probability densities. The central concept is Bayes' formula

$$p(S|D) = \frac{p(D|S)p(S)}{p(D)} \tag{2.31}$$

where the conditional probability $p(S|D)$, the posterior probability, means the probability of the solution S given the data D. Similarly, $p(D|S)$ expresses the probability of the data D given the solution S. The marginal probability $p(S)$ is the prior information about the solution S, and $p(D)$ is a normalisation constant. A solution is then extracted by applying a *point estimator* on the posterior probability $p(S|D)$. In general terms, Bayes' formula states how one would optimally update the knowledge on S after observing D.

The MEG inverse problem can be cast in the Bayesian framework. One can ask what is the probability of a certain primary current distribution given a set of MEG measurements and the prior information. Bayes' formula could be written as

$$p(\mathbf{q}|\mathbf{b}) = \frac{p(\mathbf{b}|\mathbf{q})p(\mathbf{q})}{p(\mathbf{b})} \tag{2.32}$$

where $\mathbf{q}$ is a primary current distribution, and $\mathbf{b}$ denotes the MEG measurements. The term $p(\mathbf{b}|\mathbf{q})$ is the likelihood of the measurements given the source constellation $\mathbf{q}$ and it thus embodies the forward solution; if $\mathbf{q}$ gives rise to a set of measurements similar to $\mathbf{b}$, the likelihood is high. The $p(\mathbf{q})$ contains the prior information on the sources and it could be derived from physiology, anatomy, and other imaging modalities such as fMRI (e.g. Liu *et al.*, 1998).

Dipole models

The current dipole, illustrated in Sec. 2.1.2 and defined by Eq. (2.24), serves well as a simple model of the primary current distribution provided that only one small patch of neural tissue is active at a time. A current dipole fitted to best explain the measured data is called an *equivalent current dipole*, or ECD. Since the magnetic field depends non-linearly on the dipole position, the best fit has to be obtained using non-linear minimisation algorithms that search for a minimum of a cost function by adjusting the dipole position $\mathbf{r}$ and moment $\mathbf{Q}$. The cost function is usually the sum of the squared errors between the measured $\mathbf{b}$ and estimated $\hat{\mathbf{b}}$ (via the forward solution) magnetic signal vectors, *viz.* $e = \|\mathbf{b} - \hat{\mathbf{b}}\|^2$. The validity of the dipole model can be assessed by considering the *goodness-of-fit* which is usually defined as $g = (1 - e/\|\mathbf{b}\|^2) \cdot 100\%$. However, a high goodness-of-fit does not necessarily imply that a dipole is the correct model for the underlying primary current distribution.

To relax the assumption of only a single active source at a time, the model can comprise multiple dipoles, which are fitted either simultaneously or individually to spatially filtered versions of the data. Such *multidipole models* are usually obtained heuristically by isolating the contribution of each neural source area, primarily by picking time points where the magnetic field map resembles that of a single dipole, and secondarily by selecting a subset of MEG channels and fitting a single dipole to the signals from each of these areas. Such selection of suitable dipole fitting conditions involves subjective judgement, can be labour-intensive when modelling complex source constellations, and is often cumbersome to document precisely. Subspace scanning methods such as *multiple signal classification* (MUSIC) (Schmidt, 1986; Mosher *et al.*, 1992) and its variant *recursively applied and projected MUSIC*, or RAP-MUSIC (Mosher *et al.*, 1999), seek for a multi-dipole representation of the data. In Study P1, we introduced a Bayesian algorithm that automatically obtains a dynamical multi-dipole model from a MEG data set.

In traditional spatio–temporal multi-dipole models (Scherg and von Cramon, 1985), the spatial parameters (position and orientation) are usually considered fixed whereas the time courses, i.e., the magnitudes of the dipoles as a function of time, are then computed through a *linear inverse*, since the magnetic field depends linearly on the strength of the dipoles; see Sec. 2.4.1. The signal vectors corresponding to unit-strength dipoles $d = 1 \ldots D$, at locations $\mathbf{r}_d$ with orientations $\mathbf{Q}_d$, can be obtained by Eq. (2.1) for all N channels. To obtain $\mathbf{B}(\mathbf{r})$, i.e., to solve the forward problem, either Eq. (2.30) or (2.26) in a spherical or piecewise homogeneous geometry, respectively, can be used. The signal

vectors of all dipoles $\mathbf{b}_{1\ldots D}$ can then be included as columns in a *gain matrix*

$$\mathbf{G} = (\mathbf{b}_1 \ldots \mathbf{b}_D). \tag{2.33}$$

The model for the measured data $\mathbf{y}(t)$ can now be written as

$$\mathbf{y}(t) = \mathbf{G}\mathbf{q}(t) + \mathbf{e}(t) \tag{2.34}$$

and finding the best-fitting time courses $\hat{\mathbf{q}}(t)$ corresponds to minimising $\mathbf{e}$. The problem is similar to that expressed in Eq. (2.4), and here also the least squares solution is obtained as

$$\hat{\mathbf{q}}(t) = \mathbf{G}^{+}\mathbf{y}(t). \tag{2.35}$$

Since orthogonal dipoles at the same location are characterised by orthogonal signal vectors, and because a dipole with any orientation at that location can be expressed as their linear combination, rotating sources can be embodied in the above model.

The invertibility of $\mathbf{G}$ determines MEG's spatial resolving power; if two non-orthogonal dipoles are too close to each other, the condition number of $\mathbf{G}$ is high and the estimated time courses $\hat{\mathbf{q}}(t)$ may be meaningless, showing spurious interaction of the dipoles. We encountered such a situation in P2 for the multiple dipoles confined to the brainstem; it was not possible to obtain non-interacting time courses of those dipoles. By contrast, in P3 and P4, which concentrated on cortical activity at sufficiently distant regions, the linear inverse yielded plausible time courses.

The above methods seek to represent the data with a small number of dipoles, or, in more general terms, with a small set of parameters. Hence, these algorithms are often referred to as "parametric" as opposed to "imaging" inverse modelling methods which estimate a large set of parameters to provide an image of brain activity (Baillet *et al.*, 2001). The methods described in the following Section belong to this latter class.

Minimum norm estimates

Instead of modelling the data with a small set of focal sources, one could estimate a spatial map of the activity. For such a mapping, one would distribute—without spatial fitting—a large number of dipoles throughout the brain and then obtain their strengths or time courses using the linear inversion technique described above (Eqs. 2.34 and 2.35). The *source space*, i.e., the locations of these dipoles, can either span the cranial volume

uniformly or be constrained to the cortex (Dale and Sereno, 1993) where the bulk of MEG activity originates.

However, this approach entails many more unknown dipole strengths than there are measurements, and thus $\mathbf{G}$ is not invertible. In addition, the nearby sources make $\mathbf{G}$ ill-conditioned, as explained before. Yet, a unique solution can be obtained by imposing additional constraints on the dipole strengths. A common constraint is to require that while the estimate explains the measurements, the sum (in the sense of some norm) of the dipole strengths must be as small as possible. This minimisation problem calls for two terms in the cost function; a data term that expresses the deviation of the estimate from the measurements, and a model term that describes the correspondence of the estimate to the model specified *a priori*. Adding the latter term is equivalent to applying Tikhonov regularisation. Now, the minimum p-norm version of Eq. (2.35) can be written

$$\hat{\mathbf{q}} = \arg\min_{\mathbf{q}} \{ \underbrace{\|\mathbf{W}_\mathrm{d}(\mathbf{G}\mathbf{q}-\mathbf{y})\|^p}_{\text{data term}} + a \underbrace{\|\mathbf{W}_\mathrm{m}\mathbf{q}\|^p}_{\text{model term}} \} \tag{2.36}$$

which includes the weighting matrices $\mathbf{W}_\mathrm{d}$ and $\mathbf{W}_\mathrm{m}$ for the data and model terms, respectively; a is the regularisation parameter that controls how faithfully the estimate has to follow the model. Different choices of the weighting matrices lead to different variants of the estimate; see Baillet *et al.* (2001) for a review. If both $\mathbf{W}_\mathrm{d}$ and $\mathbf{W}_\mathrm{m}$ are identity matrices and $p = 2$, this equation yields the traditional unweighted *minimum norm estimate* (MNE) (Hämäläinen and Ilmoniemi, 1984,1994). This approach tends to attribute too much of the current to the superficial dipoles as they have the strongest coupling to the sensors. To compensate for this bias, the superficial sources can be penalised by an appropriate choice of $\mathbf{W}_\mathrm{m}$, e.g., $\mathbf{W}_\mathrm{m} \propto \mathrm{diag}(g_1^{-\gamma} \ldots g_D^{-\gamma})$ where g_p's are the norms of the columns of $\mathbf{G}$ and γ is a tunable parameter. Such depth bias removal leads to *depth-weighted* or *lead-field normalised* MNE.

A modern variant of this method was applied in Study P5. To describe that method properly, the MNE approach should be re-formulated in Bayesian terms. The assumptions—in addition to those underlying the source space and its forward solution embodied in the $\mathbf{G}$ matrix—are that *i*) the source currents $\mathbf{q}$ exhibit a Gaussian amplitude distribution, *ii*) their covariance $\mathbf{C}_\mathrm{q}$ is known, *iii*) the measurement noise $\mathbf{n}$ also has a Gaussian amplitude distribution, and *iv*) the noise covariance $\mathbf{C}_\mathrm{n}$ is known. The maximum a posteriori (MAP) estimate

$$\hat{\mathbf{q}}_\mathrm{map} = \arg\max_{\mathbf{q}} p(\mathbf{q}|\mathbf{y}) \tag{2.37}$$

can then be obtained (for derivation, see e.g. Baillet and Garnero, 1997) as

$$\hat{\mathbf{q}}_{\mathrm{map}} = \mathbf{C}_{\mathrm{q}}\mathbf{G}^{\mathrm{T}}(\mathbf{G}\mathbf{C}_{\mathrm{q}}\mathbf{G}^{\mathrm{T}} + a^2\mathbf{C}_{\mathrm{n}})^{-1}\mathbf{y} \equiv \mathbf{M}\mathbf{y} \tag{2.38}$$

where $\mathbf{M}$ is the time-independent L2-norm *inverse operator*. The noise covariance $\mathbf{C}_{\mathrm{n}} = E\{\mathbf{n}\mathbf{n}^{\mathrm{T}}\}$ is typically estimated from unaveraged prestimulus baselines, from a longer block of rest data, or from a measurement without a subject. The choice depends on the experiment; for evoked responses the baselines provide the best approximation of the noise statistics, whereas for analysis of spontaneous activity the noise covariance has to be determined from data recorded in the absence of the subject since the signals of interest would otherwise be treated as noise. The full source covariance $\mathbf{C}_{\mathrm{q}}$ is practically always unknown; however, any prior information, e.g., from fMRI, about the existence of certain sources could be incorporated into $\mathbf{C}_{\mathrm{q}}$.

The MNE given by Eq. (2.38) can be converted to a dimensionless z-score by dividing the activity estimate at each source point by the estimate of noise-induced spurious activity (Dale *et al.*, 2000). This *noise normalisation* readily allows combining data across measurement modalities, e.g., EEG and MEG. As the statistics can be computed for every time sample and visualised as a map, the method is called *dynamic statistical parametric mapping* (dSPM). We applied this method in P5 to characterise the active cortical regions to our frequency-tagged visual stimulus.

The L1 norm, i.e., letting $p = 1$ in Eq. (2.36), can also be applied in MEG inverse modelling. The resulting nonlinear *minimum current estimate* (MCE) (Matsuura and Okabe, 1995; Uutela *et al.*, 1999) yields sparse, multi-dipole-like source reconstructions. However, the source time courses directly obtained from MCE often exhibit spikiness due to the nonlinearity of the estimate. Hybrid techniques have been proposed to overcome this problem (Huang *et al.*, 2006; Ou *et al.*, 2009). In Study P1, we compared the source models obtained by MCE in a previous study (Stenbacka *et al.*, 2002) with those reconstructed by the new Bayesian filtering method presented in our study.

2.4.3 Post-processing and visualisation

The source model is usually linked to the anatomy of the subject for several purposes. First, to combine data from different subjects and imaging modalities, the results should be expressed in a space that is common or transformable between the subjects and mea-

surements. In MEG, the sensor space may not be optimal for pooling data across subjects as the position of the sensor array with respect to the head typically varies across measurement sessions and subjects. Second, to maximally gain from the source models, the source estimates are typically superimposed on structural images, most often MRIs. Both tasks require co-registration of MEG and MRI, which is accomplished in three stages; prior to the MEG measurement, anatomical locations, identifiable also on MRIs, are digitised along with the locations of three or more marker coils attached on the scalp of the subject. In the beginning of the MEG recording, these coils are briefly driven by sinusoidal currents at distinct frequencies (180–200 Hz), and the emitted magnetic fields are collected for the localisation of the coils in the MEG coordinate system. By combining the information from the digitisation, one can establish a link between the head and the MEG coordinate systems (Hämäläinen *et al.*, 1993). The method has traditionally relied on the immobility of the subject's head in the MEG helmet. Recently, a system for continuous tracking and compensation of head movements has been introduced (Uutela *et al.*, 2001; Taulu and Kajola, 2005), and it has enabled measurements and accurate source analysis of otherwise challenging subject populations, such as children. However, only experienced healthy adult subjects participated in the studies in this Thesis, thus head movement compensation was deemed unnecessary.

Intersubject co-registration—mapping one person's brain to another's—poses more difficult problems. The available methods arrive at a common coordinate frame either by using gross anatomical features, such as the size of the brain, to obtain a simple and coarse coordinate transformation, or by exploiting the sulcal and gyral structure of the cortex to determine a finer-grain morphing between the brains. *Talairach transformation* (Talairach and Tournoux, 1988) is an example of the former approach, and it was employed in P2 to visualise the ECD locations in all subjects on an average brain (Collins *et al.*, 1994). The latter approach usually entails a transformation field that maps each voxel or cortical surface element to the corresponding element on the target brain. In P4, we utilised such a transformation (Schormann *et al.*, 1996; Woods *et al.*, 1998) for the whole brain volume to map the ECDs to an atlas brain (Roland and Zilles, 1996). In P5, the mapping was obtained only for the cortical surface as the MEG sources were constrained to the cortex (Fischl *et al.*, 1999).

3 Objectives

The goal of this Thesis was to develop and test methods that promise to expand MEG to new application areas. Specifically, the Thesis aimed at

- devising an automatic, principled method for determining neural generators underlying measured MEG data (Study P1),
- exploring whether deep brain areas are properly accessible by MEG (Study P2),
- investigating transient phase locking of cortical regions in response to a tactile stimulus (Study P3),
- exploring the use of stochastic resonance in a cognitive stimulus to characterise the relationship of brain and behavioural responses (Study P4), and
- characterising brain states related to subjective percepts that alternate during viewing of an ambiguous visual scene (Study P5).

4 Summary of studies

The studies comprising this Thesis are briefly reviewed here. First, the basic methodology of is summarised, and then the main motivations and results of all studies are concisely explained.

4.1 Methods

4.1.1 Subjects

The subjects in all studies were healthy adult volunteers who participated after informed consent. All recordings had prior approval by the local ethics committee. The number of subjects per study was 7–10, except in P1 where the somatosensory evoked fields for comparing the source modelling algorithms were recorded only in one subject; the algorithm of P1 was tested mostly with simulated data so that the true underlying source constellation was known.

4.1.2 Recordings

All data were collected in the MEG laboratory of the Brain Research Unit, Low Temperature Laboratory, Helsinki University of Technology, using the 306-channel MEG device (Elekta Neuromag Oy, Helsinki, Finland) with a built-in 64-channel EEG system. In that system, the helmet-shaped sensor array covers the whole scalp and comprises 102 triple-sensor elements, each housing a magnetometer and two orthogonal planar gradiometers; see Sec. 2.2. The white noise level is less than 3 $\mathrm{fT}/\sqrt{\mathrm{Hz}}$ and 3 $\mathrm{fT/cm}/\sqrt{\mathrm{Hz}}$ for the magnetometers and gradiometers, respectively. The measurements were conducted in a two-layer magnetically shielded room (ETS Lindgren Oy, Eura, Finland) supported by an active compensation system, with the compensation coils external to the room and the sensing induction coil magnetometers embedded in the walls of the room. The MEG signals were filtered to 0.1–200 Hz (to 0.03–200 Hz in P3) and sampled at 600 Hz except in P2 where the brainstem responses required a considerably wider pass-band of 0.1–1200 Hz and sampling at 3 kHz.

The stimulus generation was controlled by a personal computer running the Presenta-

tion software (Neurobehavioral Systems, Inc., Albany, CA, USA). Visual stimuli (P4 and P5) were presented using a VistaPro triple-DLP projector (Christie Digital Systems, Inc., Cypress, CA, USA) outside of the shielded room. The image was projected through an opening in the shielded room wall to a backprojection screen the subject viewed at a distance of about 1 m. Auditory stimuli (P2) were produced by a piezoelectric crystal outside of the shielded room and conveyed to the subject's ear via a plastic tube. Somatosensory stimuli (P1 and P3) were brief (0.1 ms) electric pulses delivered to the median nerve at the wrist. The output of the constant-current stimulator (Schwindt Medizintechnik GmbH, Germany) was adjusted to be slightly above the motor threshold, corresponding to a current of 5–10 mA.

The behavioural responses were collected using a silent optical switch (P5) in which the subject's finger interrupted a modulated light beam, or by a microphone recording the speech of the subject (P4). Eye tracking (P5) was performed using an infrared video camera and the associated video capturing and analysis software (SensoMotoric Instruments GmbH, Teltow, Germany). The gaze position was calibrated using 9 points at the edges of the stimulus area.

To discard data contaminated by eye blinks or gross eye movements, the vertical electrooculogram (EOG) was collected along with the MEG data; trials with the EOG variation exceeding 200 μV were rejected. Also, trials within which any of the MEG channels showed excessive variation (typically larger than 3 pT/cm in gradiometer or 5 pT in magnetometer signals) were discarded, as such large signals are most likely artefactual.

4.1.3 MRIs and co-registration

Structural MRIs were obtained with a 1.5-T MAGNETOM Vision scanner (Siemens GmbH, Erlangen, Germany) at Helsinki University Central Hospital and a 3-T Signa Excite scanner (General Electric, Inc., Milwaukee, WI, USA) at the Advanced Magnetic Imaging Centre of Helsinki University of Technology. The 3D MPRAGE (magnetisation prepared rapid gradient echo) and SPGR (spoiled gradient recalled) sequences were used to acquire the images. The approximately 1-mm^3 cubical voxels covered the whole head to enable accurate co-registration. The head coordinate system was defined on the MRIs primarily using three landmarks (pre-auricular points and nasion), but the registration was fine-tuned using digitised points (typically 40–60) across the scalp and around the nose. In the MEG system, the transformation to the head coordinate system was obtained using

four marker coils attached to the scalp of the subject; two on the forehead and two behind the earlobes. The locations of these coils and the extra points were digitised with respect to the landmarks prior to the MEG measurement using a 3D digitiser (Polhemus Navigation Sciences, Inc., Colchester, VT, USA). Tests with a phantom have indicated that the overall localisation accuracy of ideal dipolar sources is typically 2–3 mm, largely due to co-registration errors (author's unpublished data).

For obtaining the origin of a spherical conductor model and for superimposing the ECD locations on the anatomy, the co-registered 3D MRIs were used as such in P1 and P3. For P2, which required a multi-compartment conductor model, the MRIs were segmented for the cranial, skull and scalp compartments by the FreeSurfer software (Fischl *et al.*, 2004), which also established a Talairach transformation to the MNI305 average brain (Collins *et al.*, 1994). In P4, the individual MRIs underwent a combination of an affine (Woods *et al.*, 1998) and an elastic (Schormann *et al.*, 1996) transformation to map the sulcal/gyral structure of each individual subject to an atlas brain, thus allowing visualisation of the ECDs of all subjects in a common space. The cortical mantle was segmented in P5 by FreeSurfer (Fischl *et al.*, 2001) for a cortically-constrained source model, for visualisation and for morphing the source models to a common brain (Fischl *et al.*, 1999).

4.1.4 Signal processing

Residual magnetic interference was attenuated by signal-space projection (SSP) (Uusitalo and Ilmoniemi, 1997; Parkkonen *et al.*, 1999) in P2, P3 and P4, and by signal-space separation (SSS) in P1 and P5 (Taulu and Kajola, 2005). Time-domain averaging of brain responses to individual stimuli was utilised in P1–P4 to obtain auditory, somatosensory and visual evoked fields. The number of accepted trials was typically about 80–120, but the weak brainstem responses (P2) required averaging of about 16,000 trials per subject.

The oscillatory components in the recorded brain signals were isolated by 7-cycle Morlet wavelets in P3 and P5, and also by the GLM-based method (see Sec. 2.3) in P5.

4.1.5 Source modelling

The traditional multidipole approach for modelling the neural sources was applied in P1 (for comparison), P2, P3 and P4. Single dipoles were fitted to the data at time points

where dipolar field patterns were present. If multiple such patterns were present simultaneously, the fit was restricted to one at a time by selecting a group of at least 20 channels around the local signal maximum at the planar gradiometers. The fits were validated by requiring that the goodness-of-fit exceeded 70–80% and that the dipole location corresponded to the field pattern. After these spatial fits, except in P2, the source time courses were computed using all channels in the linear inversion (see Sec. 2.4.2), keeping the dipole locations and orientations fixed.

Instead of ECDs, dynamic statistical parametric mapping (dSPM) was employed in P5. The data for estimating the noise covariance were recorded with the subject present but in the absence of the dynamical stimulus, thus ensuring that the spontaneous brain rhythms were treated as noise in this case.

4.2 Dynamical MEG source modelling (P1)

As explained in Sec. 2.4.2, inferring the neural sources underlying the measured MEG data requires explicit models of the activity. Most of the existing source modelling methods do not take advantage of the temporal continuity of the activations, but either model each time point separately or use only statistics obtained across the whole analysis period. As a corollary, those methods implicitly assume that the reconstructed sources exist either throughout the analysis period or only at a single time point; the sources may show only small amplitudes at time points when they are considered "silent" but they nevertheless exist in the model. To address these shortcomings, in this study we proposed a conceptually different, dynamical model in which the sources can emerge and disappear in the course of time. Then, questions such as how many distinct local sources exist at a given time point can be readily answered. In addition, we exploited the continuity of the brain responses by using the statistics of the source configuration at the previous time point as the prior information for the next time point. The problem was solved in the Bayesian framework, which also allows incorporating other prior information, such as data from other imaging modalities.

The algorithm is a sequential Monte-Carlo filtering process which tries to find the best-fitting multidipole model for each time point. A large number of candidate multidipole models are expressed as *particles* (for a review of particle filtering, see Arulampalam *et al.*, 2002). Each particle holds the parameters $\mathbf{r}_{1\ldots D}$ and $\mathbf{Q}_{1\ldots D}$ of one complete D-dipole model (see Sec. 2.4.2), where D can differ across particles. Each particle is assigned a

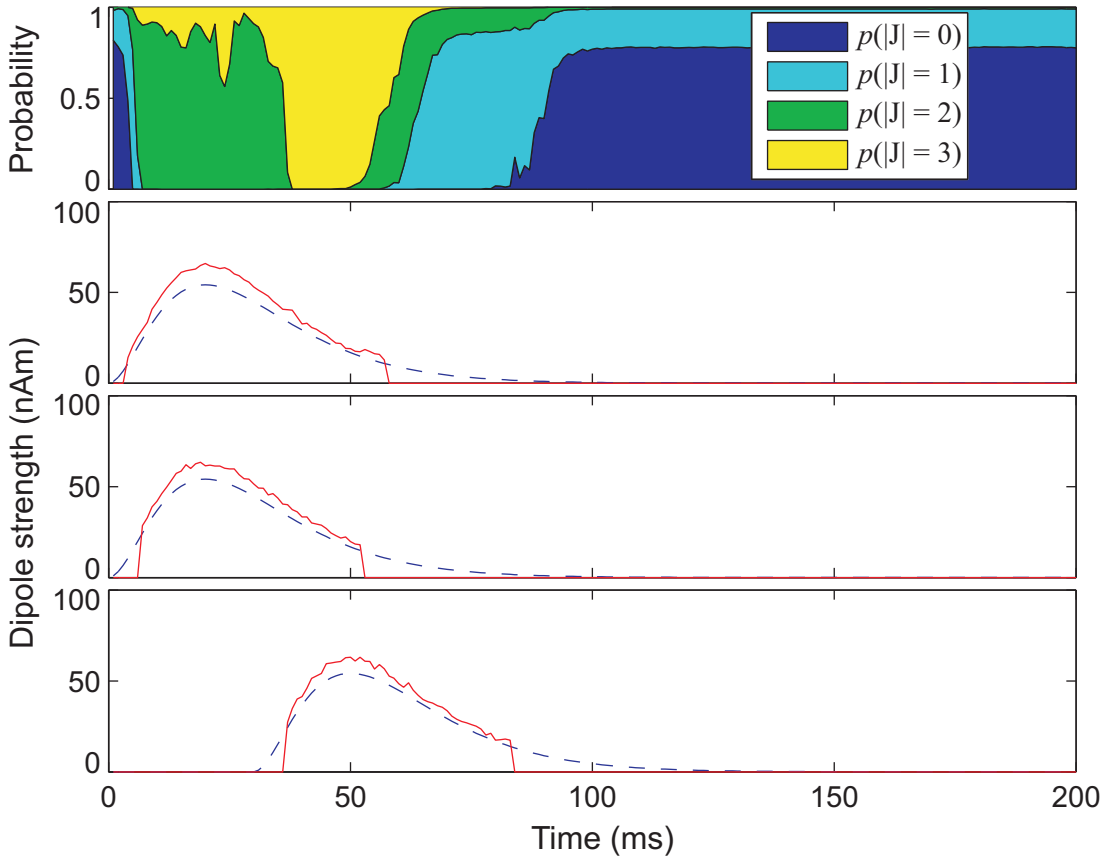

Figure 4.1 A source reconstruction by the Bayesian tracking algorithm of P1. Three simulated current dipoles (blue dashed lines), two of which were fully correlated in time, and their reconstructed dipole strengths (red solid lines). The model selection, i.e., the probabilities of different numbers of sources (top panel). *An unpublished result of the authors of P1.*

weight proportional to the likelihood of the corresponding model given the measured data. Thus, the particle set approximates the instantaneous probability distribution of the source space.

The data are sequentially analysed by employing the posterior distribution obtained at time t as the prior distribution at $t+1$ via the Chapman–Kolmogorov equation and taking into account the likelihood, i.e., the match with the measurements, using Bayes' formula (Eq. 2.31). A new set of particles is extracted according to the likelihoods and this set is subjected to an evolution process where random perturbations to the dipole parameters likely yield a subset of particles which are even better fit to the data at this time point. The process is then repeated for each time point within the analysis window, always using the

obtained posterior distribution as the prior distribution for the next time step. Since the probability distributions as such cannot be used as source models, a *probability hypothesis density* (PHD) (Mahler, 2003) was computed to retrieve the most likely source constellation for each time point. Since the particles representing the "best" source models are generally different for each time point, clustering by location, orientation and time of occurence was a necessary post-processing step to group together the dipoles that reflect a certain neural source; otherwise it would not be possible to determine the time course of each source. Despite the clustering, the sources may still move, emerge and disappear during the analysis period. Figure 4.1 illustrates the result from a simple three-dipole simulation.

In P1, the algorithm was tested with Monte-Carlo simulations, with simulated data mimicking hypothetical responses to a complex visual stimulus (Stenbacka *et al.*, 2002), and finally with real data from a somatosensory experiment. In comparison with traditional multidipole modelling and MCE, this new Bayesian filtering algorithm displayed similar or slightly better performance in terms of the accuracy of the source reconstruction, achieved fully automatically, without subjective judgement on the existence of a source or expert knowledge as to the brain areas active in a given task.

4.3 Magnetic auditory brainstem responses (P2)

Deep brain areas, such as the thalamus and brainstem, are traditionally considered unreachable by MEG due to their depth and the associated reduction in signal amplitude, but also due to the smaller neural assemblies and their less optimal spatial arrangement compared to the pyramidal cells in the cortex. Reports on MEG measurements of such deep sources exist (e.g. Erné *et al.*, 1987; Iramina and Ueno, 1995; Tesche, 1996; Lütkenhöner *et al.*, 2000); however, in these studies source localisation was either severely hampered by the low signal-to-noise ratio or the location was assumed based on the anatomy and then used as a spatial filter. Here, we showed that magnetic auditory brainstem responses (mABRs) can be recorded in such a way that reliable, data-driven source modelling is possible (Fig. 4.2). A large array of low-noise magnetometers and an interference suppression system that did not attenuate signals from deep sources were instrumental in obtaining data with an adequate SNR. Equally important was a robust neural response whose frequency content was separable from that of the cortical activity, thus allowing suppression of strong cortical signals by simple filtering.

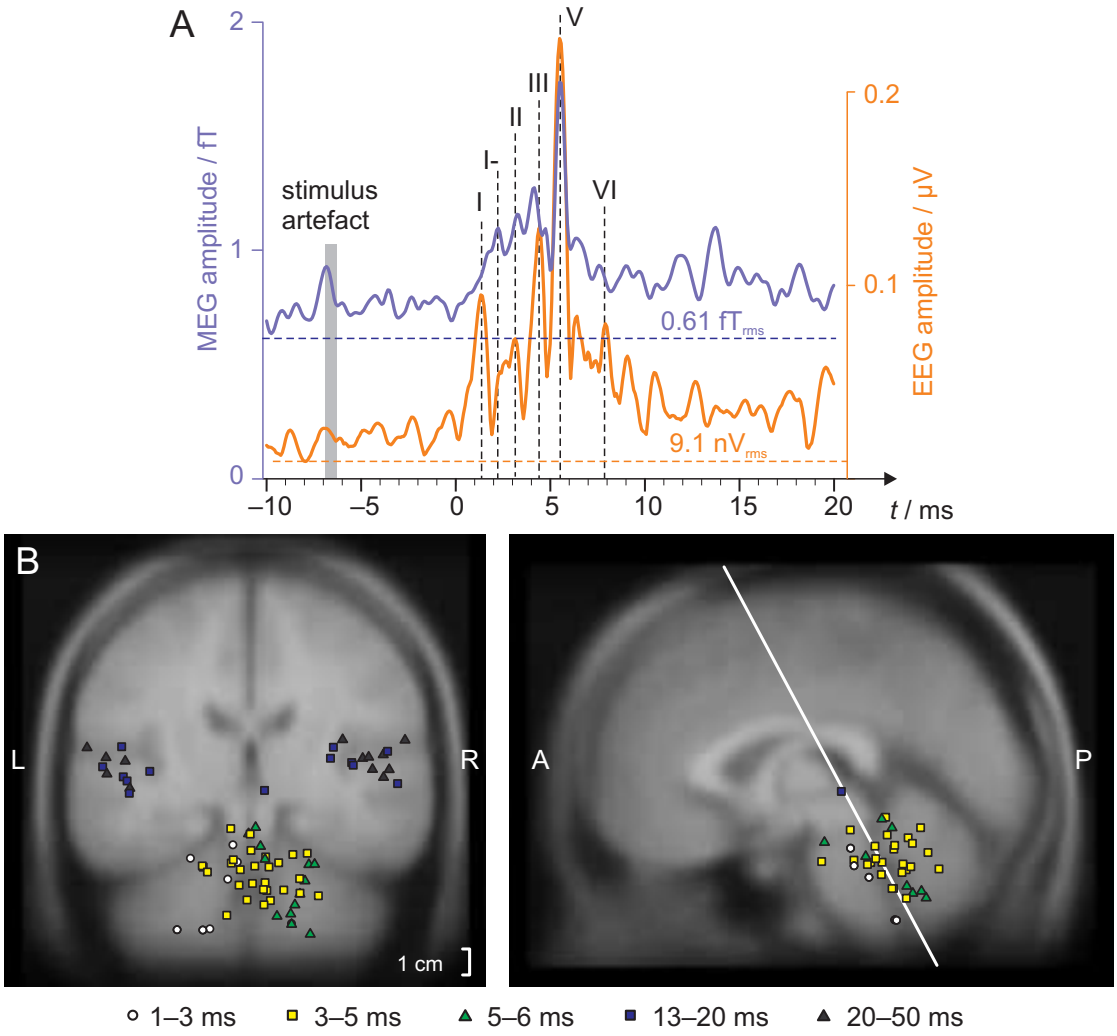

Figure 4.2 Auditory brainstem responses. **A** Grand averages of magnetic and electric responses across all subjects ($N = 7$; latencies adjusted so that individual wave-V responses overlapped) and all magnetometer channels (root-mean-squared) of the data filtered to 180–1000 Hz. The roman numerals denote the ABR deflections. Intrinsic MEG and EEG system noise levels, taking into account the number of trials averaged, are indicated by the dashed horizontal lines. **B** ECD source locations in all subjects. Dipole locations were Talairach-transformed, colour-coded for latency, and superimposed on the MNI305 average brain. *Adapted from P2.*

The auditory brainstem response (ABR) (Jewett *et al.*, 1970) comprises five to seven brief responses, "waves", within 10 ms after a presentation of a click tone. The first two waves originate in the auditory nerve whereas waves III–V are generated within the brainstem (Møller, 2007). Although wave V typically has the largest amplitude of all ABR waves, its laterality has been disputed. Lesion (Markand *et al.*, 1989) and PET (Giraud *et al.*, 2000)

studies have suggested an ipsilateral origin of wave V whereas, e.g., subdural recordings from the basal temporal surface (Zappia *et al.*, 1996) indicated a contralateral origin. Our study strongly suggested contralateral generation of wave V. Since the electric auditory brainstem responses and particularly wave V are utilised clinically for diagnosing pathologies in the early auditory pathway, this confirmation likely increases the value of such use.

We employed a realistically-shaped three-compartment boundary element model in the forward modelling. Since many of the sources were in the vicinity of tissue-type boundaries, a more accurate model taking into account the different conductivity of the cerebrospinal fluid in the ventricles, for example, might have improved the localisation results further. Anisotropic conduction could also play a more significant role here than in studies of cortical activity, and thus a finite element model of the volume conductor (Wolters *et al.*, 2006) would be appropriate if accurate anatomical data were available for such a model.

4.4 Phase locking between primary and secondary somatosensory cortices (P3)

Rhythmic brain activity has been postulated to convey information in its phase (see e.g. Engel *et al.*, 2001; Varela *et al.*, 2001). The central idea is that the impact or purpose of a neural event could differ depending on its timing with respect to the phase of a large-scale oscillation.

Both the primary (SI) and secondary (SII) somatosensory cortices show evoked responses to somatosensory stimuli (Hari and Forss, 1999). Thus, SI and SII share information about the stimulus, either via a direct connection between the cortices or indirectly via, e.g., thalamus. In this study, we tested whether such information transfer could happen, at least partially, as transient phase locking. Specifically, we examined the oscillatory components for a consistent phase difference between the signals from the SI and SII cortices in response to sensory input, in this case a brief electric stimulus to the median nerve at the wrist. The instantaneous phase locking was quantified by computing the PLV; see Sec. 2.3.2. Such phase locking was found in most subjects at around 20 Hz, 80–90 ms after the stimulus, between the contralateral SI and ipsilateral SII cortices. Figure 4.3 shows the PLV of one subject. Our data suggested similar locking between

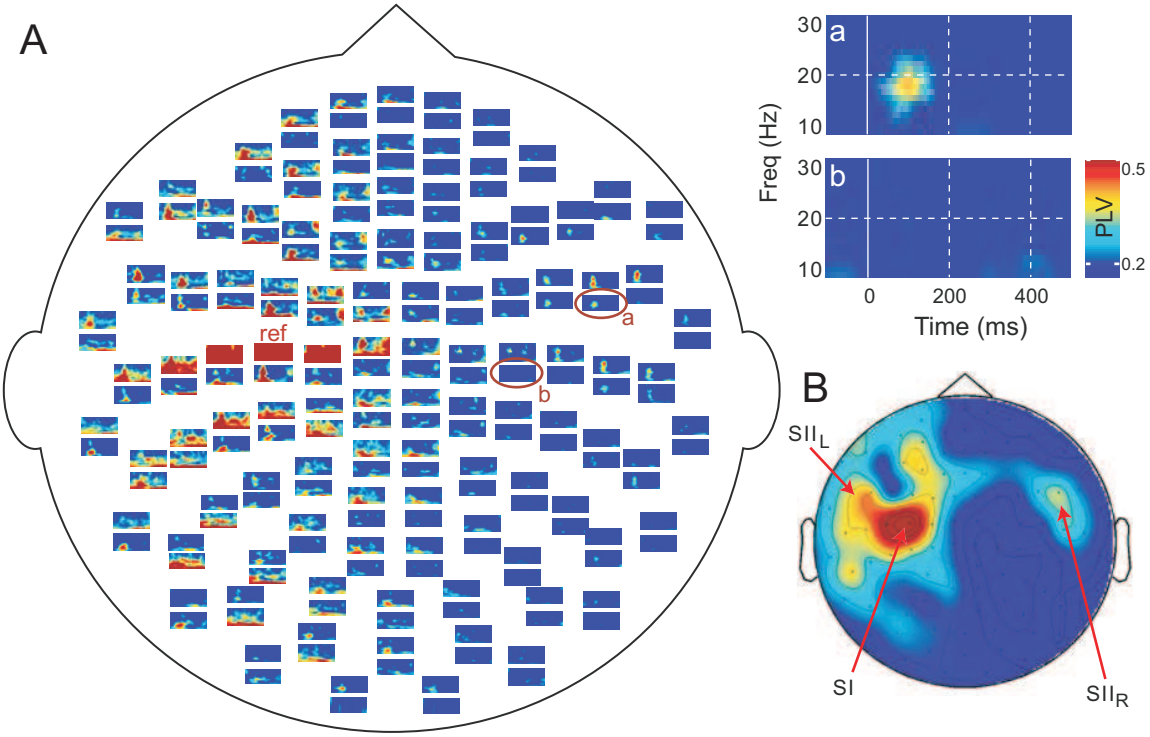

Figure 4.3 Phase locking between SI and SII cortices in one subject. **A** Time–frequency representations of the PLVs computed for all planar gradiometer channels, using data from the channel above the contralateral SI as the reference signal. **B** A topographic representation of PLV distribution at 18–22 Hz, averaged across 50–150 ms post-stimulus. *Reprinted with permission from P3.*

the contralateral SI and SII cortices as well, but we could not completely exclude the possibility of cross-talk at the sensor level. Statistical testing was instrumental in this study as merely the evoked responses could give rise to the observed phase-locking; using the PLS method with surrogate data (see Sec. 2.3.2) to establish the level of stimulus-locked and spurious phase locking, we showed that most of the observed phase locking is stimulus-induced, i.e., not due to the responses tightly locked to the stimulus.

4.5 Stochastic resonance in visual stimulation (P4)

Stochastic resonance (SR) is a phenomenon in which adding an appropriate amount of uncorrelated noise to a subthreshold stimulus allows its detection. This, perhaps counterintuitive, effect can be explained as a combination of two steps: first, the added noise increases the amplitude of the subthreshold signal so that it occasionally exceeds the

threshold, leading to a stochastic train of suprathreshold impulses. Second, this impulse train is low-pass filtered, which yields a moving-average amplitude that reflects the amplitude of the original, noiseless stimulus. In other words, temporal resolution is traded for better amplitude resolution. SR was first proposed for modelling physical systems but was later discovered in neural systems (Longtin *et al.*, 1991; Anderson *et al.*, 2000); for a review, see Moss *et al.* (2004).

We devised an experiment in which a visual stimulus exhibited SR in such a way that the subthreshold part formed a written word. The amplitude of added dynamic noise was then varied around the resonance, defined to give the maximum contrast between the word and the background at the limit of infinite exposure time. Our experimental design differed from previous work utilising varying amounts of superimposed noise (e.g. Tarkiainen *et al.*, 1999) by featuring this resonance, which was reflected in both the source amplitudes and behavioural results.

The evoked responses to the word onset displayed different sensitivities to the amount of added noise: the early visual responses in the occipital cortex depended most strongly on the noise level whereas the late, N400-type responses in the temporo–parietal cortex, showed a broader peak around the resonance. Behavioural data on the word detection rate correlated best with these late responses, supporting their relation to the processing of the semantic content of the stimulus words (Kutas and Hillyard, 1980; Helenius *et al.*, 1998).

4.6 Frequency-tagging approach to study bistable visual perception (P5)

Ambiguous figures that allow for two interpretations often trigger spontaneous switching between the percepts. This bistability of perception is stochastic although it can be biased by manipulating the stimulus (Leopold *et al.*, 2002; Sterzer and Rees, 2008). The perceptual alternations may manifest the reconciliation of the sensory input and the prior information on the structure of visual scenes, and in the case of these figures, the two outcomes are equally likely. If one considers the perceptual apparatus as a Bayesian inference machine (Lee and Mumford, 2003), an ambiguous scene corresponds to a bimodal posterior distribution. Then, even subtle variations may perturb the system to switch from one state to the other. These perturbations are likely intrinsic to the brain as the switches occur without any changes in the physical stimulus or in the sensory organs.

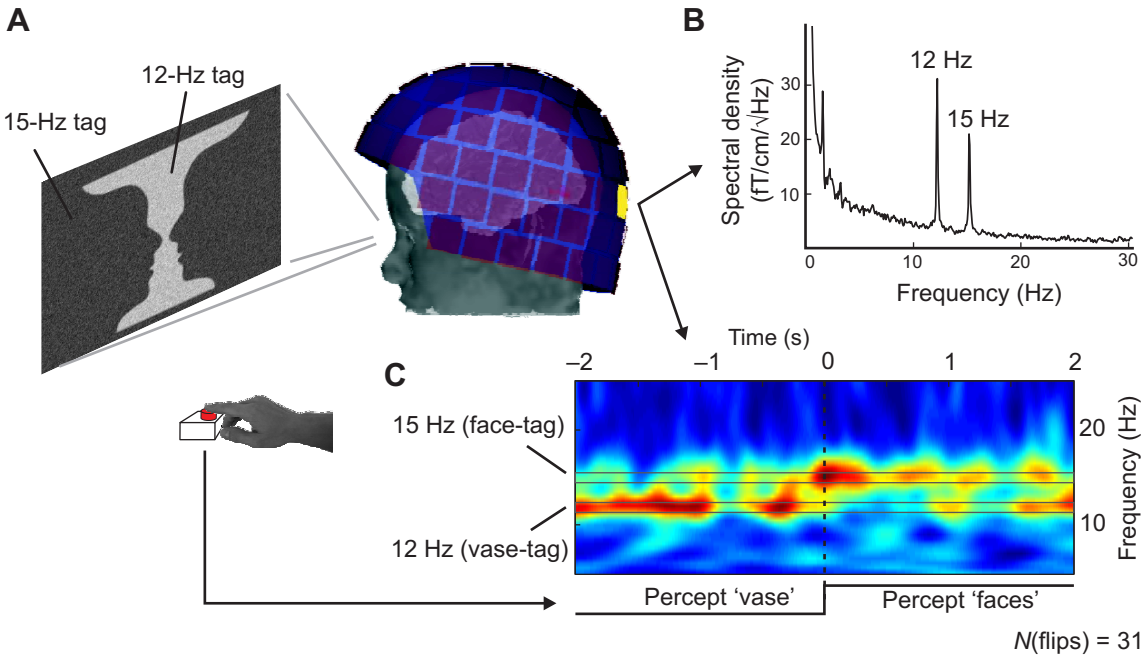

Figure 4.4 Investigating bistable visual perception with a frequency-tagged stimulus. **A** Dynamic noise at two update frequencies superimposed on Rubin's face–vase figure. **B** A spectrum of an occipital MEG sensor showing the tag-frequency peaks. **C** A time–frequency representation of the power at these frequencies around the behaviourally-reported perceptual switch. *Reprinted with permission from P5.*

We wanted to investigate how the brain activity differs during the two percepts of Rubin's face–vase figure. Evoked responses could not have illuminated this question, but they—both hemodynamic and electrophysiological—have been used to study the perceptual switch itself (Kleinschmidt *et al.*, 1998; Pitts *et al.*, 2008). To monitor the maintenance of and the difference between the brain states related to perceptual states, we superimposed regional marker signals, tags, on the stimulus image. The vase area was tagged with a subtle noise pattern oscillating at 12 Hz while the rest of the image was tagged with a similar pattern oscillating at 15 Hz; see Fig. 4.4. The noise was not perceptually salient and the spontaneous switching of the percepts was preserved. Recording the 12- and 15-Hz signals from the brain allowed us to determine at least some of the brain areas where the stimulus was processed and to follow the relative strengths of these processes as a function of the perceptual state, which the subjects reported behaviourally.

In all subjects, the early visual areas displayed tag-related activity; primary visual cortex V1 showed the largest contribution. In some subjects, lateral occipital areas also elicited

12/15-Hz signals when the subject was viewing the tagged stimulus. Owing to their relatively high temporal frequency, the tags did not penetrate much further in the hierarchy of visual brain areas. However, importantly, the balance of these signals from V1/V2 varied according to the subjective percept, indicating that the activity in V1/V2 covaries with the perceptual state, despite the invariant feedforward input to V1. These modulations likely result from the feedback activity from higher-order visual cortices, and they may serve in figure–ground segregation by accentuating the figure part (Lamme, 1995) and also—in more general terms—in the selection of the relevant parts of the visual scene for spatial attention (Saalmann *et al.*, 2007).

The source of the top-down modulations remains elusive. The modulations may be associated with the selection of goal-directed behaviours (Leopold and Logothetis, 1999; Lumer *et al.*, 1998; Windmann *et al.*, 2006) or simply be a manifestation of brain's mechanism to avoid locking to a single interpretation in an ambiguous situation (Leopold and Logothetis, 1999).

5 Discussion

The primary aim of this Thesis was to expand the applicability of magnetoencephalography in studies of human brain function. Compared with other available non-invasive methods, MEG presents a unique combination of excellent temporal and reasonable spatial resolution. Indeed, the temporal and spatial dimensions should be considered together. The ability to track a specific neural population in time often entails spatial localisation of that population and isolation of its contribution to the measurements. On the other hand, one can search for activations in space that exhibit certain temporal characteristics, such as oscillations at specific frequencies. In addition, spatial localisation can benefit from the temporal continuity of the neural activations. Taken together, the temporal aspect that MEG provides with respect to, e.g., fMRI offers more than just one additional dimension.

5.1 Benefits of spatio-temporal approaches

To fully exploit the joint spatio-temporal information in the MEG data, the analysis methods should take both sides into account. The Bayesian filtering method presented in Study P1 allows that explicitly; the algorithm includes an *a priori* evolution model that can capture the typical temporal behaviour of a neural source and takes advantage of the predictions of that model when searching for the spatial parameters of the sources. Similarly, the obtained source reconstruction is not spatially static as in most other source modelling methods, but also the spatial arrangement can evolve in time. With our relatively uninformed evolution model, which only exploited the temporal continuity of the neural activations, the method presented in P1 attained similar reconstruction accuracy as obtained by multi-dipole modelling and MCE performed by scientists with varying expertise in source modelling (Stenbacka *et al.*, 2002). Since the method presented here is fully automatic, the demonstrated performance can be considered better than that of the human-assisted methods. In addition, since the applied priors were rather uninformative, better results are to be expected when more physiological and anatomical information is included.

A precursor of the Bayesian filtering method in P1 has been compared by Pascarella *et al.* (2007) with other automatic source modelling methods using simulated data with

dipolar sources : RAP-MUSIC (Mosher *et al.*, 1999) performed in a comparable manner with both correlated and uncorrelated stationary sources, but it was inferior if the true sources moved, causing RAP-MUSIC to reconstruct a number of sources with different time courses. Bayesian filtering captured the moving source as one since the source model is dynamical, that is, the filtering algorithm also updates the spatial parameters of the model at every time step. On the other hand, RAP-MUSIC was considerably faster to compute.

The combined spatial and temporal information of MEG was also directly utilised in Studies P3 and P5, where cortical regions were identified based on the temporal structure of the signals they emitted. With respect to EEG, MEG's spatial localisation power was instrumental in the study of cortico-cortical phase-locking (P3); in EEG, a reliable separation of signals from the somatosensory cortices would have been a challenging task, whereas such a separation was straightforward in MEG with the focal planar gradiometer channels, even without an explicit source model.

Stochastic resonance (SR) successfully worked as a way to parametrise the stimulus. Contrary to simply superimposing a varying amount of noise, the SR design of Study P4 allowed increasing and decreasing the signal-to-noise ratio while maintaining a qualitatively similar noisy appearance of the stimulus. The cortical activation chain had a successively weaker dependence on the noise level, approaching that of the behavioural performance. This approach could potentially be systematised to parcel out the source regions directly from, e.g., a minimum norm estimate.

5.2 Expanding the frequency regime

Traditionally, MEG and EEG studies have concentrated on cortical responses whose frequency content is below 100 Hz; the same has been true for both evoked responses and oscillatory activity for the simple reason that the great majority of all activity recorded with these two methods is confined to that frequency range. Yet, responses at much higher frequencies have been detected. For example, the SI cortex is known to generate short bursts of MEG and EEG activity at around 600 Hz in response to electric median nerve stimulation (Curio *et al.*, 1994; Hashimoto *et al.*, 1996). In addition, intracranial EEG has indicated that epileptogenic tissue generates signals at 80–500 Hz (Bragin *et al.*, 1999; Jacobs *et al.*, 2009); however, such activity has not yet been demonstrated in scalp EEG or MEG, likely due to the weakness of these signals, combined with the lack of a

phase-locked reference signal to trigger response averaging.

Deep brain areas can generate high-frequency activity that is detectable non-invasively; the auditory brainstem responses, first shown in scalp EEG (Jewett *et al.*, 1970) and demonstrated here with MEG in Study P2, extend above 1 kHz in frequency. The frequency content plays a major role in the detectability of these responses as they would easily be masked by cortical activity that can be an order of magnitude stronger and is much easier to detect by the sensor array due to the shorter source–sensor distance. However, the cortical contribution falls off rapidly with increasing frequency (see Fig. 2.3 for a spectrum of total MEG activity), thus high-pass filtering can be applied to effectively suppress the bulk of the cortical signals. Yet, the possible low-frequency activity of deep structures remains obscured by the cortical activity. In principle, accurate source modelling of the cortical activity would allow its removal from the data but since even the activity uncorrelated and independent of the stimulus or task likely acts as a mask, such modelling would be very demanding in most cases.

Detection of these high-frequency responses depends crucially on the system noise level. Since the instrumentation and the background brain activity are uncorrelated noise sources, their contributions add quadratically, and therefore the larger by far dominates. The brain contribution is larger than the system noise level at frequencies upto about 100 Hz, above which the system is the major source of noise[3]. Further reduction of the system noise level would thus clearly improve the visibility of brain signals above 100 Hz. Such developments would increase MEG's utility in investigating both deep activations with associated high-frequency components and superficial neural sources that exhibit the high-frequency oscillations mentioned above. On the other hand, the signal-to-noise ratio of the traditional low-frequency responses is limited mainly by the on-going background brain activity, "brain noise", and within that regime the advantage of a considerably lower system noise level is questionable. The ultimate limit is set by the magnetic noise due to the thermal motion of charge carriers in the body, estimated to be on the order of 0.1 $\mathrm{fT}/\sqrt{\mathrm{Hz}}$ at the measurement distance of 5 mm (Varpula and Poutanen, 1984). Instrumentation noise is still far above.

The frequency axis can also be expanded towards very low frequencies. Near-DC or infraslow phenomena have been recorded by MEG (Cohen *et al.*, 1980; Barkley *et al.*, 1991; Mackert *et al.*, 2001). DC-MEG recordings seem to yield important neurophysio-

[3]The white noise level of today's state-of-the-art MEG systems is about 3 $\mathrm{fT}/\sqrt{\mathrm{Hz}}$, and the total noise is approximately $\sqrt{2}\cdot 3\ \mathrm{fT}/\sqrt{\mathrm{Hz}}$ at 100 Hz; see Fig. 2.3

logical data, similarly as DC-EEG, or full-band EEG, has done (Vanhatalo *et al.*, 2004). Long, sustained responses recordable with DC-MEG allow fMRI-like experimental designs, where active (task or stimulation) and rest periods alternate (e.g. Lammertmann and Lütkenhöner, 2001).

5.3 Employing temporally-structured stimuli

Study P5 rested on the cortical responses to the temporal structure of the stimulus itself; the faint frequency tags present in a visual stimulus were reflected in the activity of the early visual cortices. A similar approach but with a salient flickering stimulus has been applied to study binocular rivalry using EEG (Lansing, 1964) and MEG (Tononi *et al.*, 1998; Srinivasan *et al.*, 1999). In the auditory modality, frequency tagging has been introduced to monitor the contributions of the two ears to the activity in both auditory cortices during binaural listening (Fujiki *et al.*, 2002; Kaneko *et al.*, 2003), and recently to study word learning while listening to continuous speech (Buiatti *et al.*, 2009). Stimulus tagging could also be employed in fMRI but the slowness of the hemodynamic response severely limits the usable tag frequencies. Multifocal approaches to human vision, applicable both to fMRI (Vanni *et al.*, 2005) and EEG (Sutter, 2001), also rely on temporally structured stimuli to highlight brain areas that respond, e.g., to a certain location in the visual field. However, multifocal experimental designs evoke transient responses whereas tagged stimulation is usually continuous and elicits continuous oscillatory or steady-state responses. Thus, tagging is better suited for studying on-going processes, such as the maintenance of a perceptual state.

In previous frequency-tagging experiments, the tags have been perceptually salient to ensure a high signal-to-noise ratio of the tag-related signals from the brain. While large signals are desirable, the distinct flickering or hum are usually not, as they may severely degrade the actual content of the stimulus. To circumvent this problem, in Study P5 we developed a new tag: dynamic noise superimposed on the stimulus image. That tag was only mildly perceivable while still eliciting relatively large tag-related oscillatory signals in the early visual areas. Importantly, the stimulus feature of interest—spontaneously switching percepts to an ambiguous figure—was preserved.

The tag frequency has to be selected carefully. Tagging with a low frequency (< 10 Hz in a visual stimulus) corresponds to an evoked response study and often gives rise to harmonic components in the tag-related signal, which may complicate the analysis. Higher

tagging frequencies do not generate harmonics but the signal amplitude at the fundamental frequency decreases as well, and the tag may not propagate as far in the hierarchy of cortical regions due to the different recovery cycles of different cortical regions (Uusitalo *et al.*, 1996). For extracting the tag-related signals from the MEG data, the model-based detection (see Sec. 2.3.2) was more flexible than Fourier transform-based approaches as it was not restricted to orthogonal frequencies.

5.4 Clinical and neuroscientific implications

Modelling the neural sources underlying MEG responses can be elaborate and time consuming. Further development of the automatic algorithm introduced in Study P1 can provide means to capture the essentials of the data without human intervention, which would be beneficial particularly in clinical MEG, where the time allocated for analysis is often limited. The target-tracking nature of the algorithm lends itself to real-time analysis of brain activity; learning the statistical properties of the source constellation should improve the attainable signal-to-noise ratio of single responses, which may open up new ways to provide biofeedback or otherwise alter the experiment in the course of the measurement. However, as of now, the computational demand of the algorithm is too high for real-time use.

The success in recording and modelling neural generators in the brainstem suggests that other activity below superficial brain areas may also be accessible by MEG. Recording and localising epileptic spikes in the mesial temporal cortex is possible with a similar magnetometer array as used in our study (Enatsu *et al.*, 2008). Also, a recent simulation study supported the visibility of signals from basal ganglia and hippocampi in MEG (Attal *et al.*, 2007). Together, these studies indicate that at least high-frequency activity in the deeper structures can be recorded and localised with MEG, which should improve the clinical utility of MEG further. In the light of these results, recording thalamic and hippocampal signals can be considered more feasible than before, even without strong spatial priors in the source analysis.

The role of cortical oscillations in information transfer was supported by the transient phase-locking of the SI and SII cortices in Study P3. However, the mere synchronisation does not ascertain that these areas communicate directly with each other. In addition to the cortico-cortical connection from the SI cortex, the SII cortices also receive thalamic projections; it is thus plausible that the thalamus could drive both cortical regions with

an oscillatory signal. One could speculate that—analogously to the postulated role of gamma oscillations for binding different visual features (for reviews, see e.g. von der Malsburg, 1999; Engel and Singer, 2001)—such a thalamo-cortical signal could serve as a mechanism to bind together the transient representations of the stimulus features in SI and SII cortices for a unified percept.

Study P5 revealed that during bistable visual perception, the subjective perceptual alternations are associated with corresponding changes in the activity of the early visual areas, presumably V1 and V2. These activity changes are likely due to top-down feedback, which further supports the notion that activity in early visual areas is not just a feedforward reflection of retinal input. This finding endorses the active role of V1/V2 in visual awareness, contrary to some earlier views which attributed conscious vision only to the higher-order visual cortices (Crick and Koch, 1995).

5.5 Future directions

MEG's excellence in temporal resolution combined with reasonable spatial accuracy makes MEG the tool of choice for investigating cortical oscillations *per se* and the functional connectivity mediated by these oscillations. On the other hand, the same combination should also help track the neural processing of continuous, possibly even natural stimuli. Should these kind of approaches succeed, they may trigger a paradigm shift in neuroscience from applying highly controlled, simplistic stimuli to real-life-like multimodal scenarios. As an intermediate solution towards more complex stimuli, the non-salient stimulus tagging developed in this Thesis could be explored further; for example, non-periodic tags could be even less perceivable, particularly in the auditory modality, and they might allow further probing of the cortical areas. If evoked responses are viewed as manifestations of prediction updates concerning the surrounding world (Friston, 2005), tagging can provide access to some of the brain states, i.e., the results of those predictions.

6 Conclusions

The aim of this Thesis was to advance MEG to realms that have been considered difficult or even impossible for it. Specifically: *i*) A Bayesian tracking algorithm was introduced to automate MEG source modelling and to allow principled inclusion of prior anatomical and physiological information. The performance of the algorithm was comparable to previous human-assisted methods. *ii*) Neural activity in the brainstem was successfully recorded and accurately localised, which also supports MEG's clinical utility when investigating deep brain areas. *iii*) Oscillatory 20-Hz signals from the primary and secondary somatosensory cortex were shown to be transiently phase-locked to tactile stimuli, possibly signifying functional connectivity between those areas. *iv*) Using a stimulus exhibiting stochastic resonance, a systematic quantification of the correlations between stimulus parameters, brain signals and behavioural performance was possible. *v*) A new frequency-tagging method to separate brain activations elicited by different parts of a visual scene was developed and applied to probe the neural engagement in the early visual brain areas during bistable perception. Recordings revealed that already the early visual areas reflect the subjective percept. The finding supports the active role of the early visual areas in conscious vision. The results obtained in this Thesis present methodological advances that likely contribute to future applications of MEG in basic and clinical neuroscience.

References

Abascal JPJ, Arridge SR, Atkinson D, Horesh R, Fabrizi L, De Lucia M, Horesh L, Bayford RH, Holder DS (2008). Use of anisotropic modelling in electrical impedance tomography: description of method and preliminary assessment of utility in imaging brain function in the adult human head. *Neuroimage* 43: 258–268.

Ahlfors SP, Ilmoniemi RJ, Portin K (1993). The effect of stimulation rate on the signal-to-noise ratio of evoked responses. *Electroencephalogr Clin Neurophysiol* 88: 339–342.

Ahlfors SP, Simpson GV (2004). Geometrical interpretation of fMRI-guided MEG/EEG inverse estimates. *Neuroimage* 22: 323–332.

Ahonen AI, Hämäläinen MS, Ilmoniemi RJ, Kajola MJ, Knuutila JE, Simola JT, Vilkman VA (1993a). Sampling theory for neuromagnetic detector arrays. *IEEE Trans Biomed Eng* 40: 859–869.

Ahonen AI, Hämäläinen MS, Kajola MJ, Knuutila JET, Laine PP, Lounasmaa OV, Parkkonen LT, Simola JT, Tesche CD (1993b). 122-channel SQUID instrument for investigating the magnetic signals from the human brain. *Phys Scripta* T49: 198–205.

Akhtari M, Bryant HC, Mamelak AN, Flynn ER, Heller L, Shih JJ, Mandelkern M, Matlachov A, Ranken DM, Best ED, DiMauro MA, Lee RR, Sutherling WW (2002). Conductivities of three-layer live human skull. *Brain Topogr* 14: 151–167.

Anderson JS, Lampl I, Gillespie DC, Ferster D (2000). The contribution of noise to contrast invariance of orientation tuning in cat visual cortex. *Science* 290: 1968–1972.

Arulampalam M, Maskell S, Gordon N, Clapp T (2002). A tutorial on particle filters for online nonlinear/non-Gaussian Bayesian tracking. *IEEE Trans Sig Proc* 50: 174–188.

Attal Y, Bhattacharjee M, Yelnik J, Cottereau B, Lefevre J, Okada Y, Bardinet E, Chupin M, Baillet S (2007). Modeling and detecting deep brain activity with MEG & EEG. In: *Engineering in Medicine and Biology Society, 2007. EMBS 2007. 29th Annual International Conference of the IEEE*, pp. 4937–4940.

Baillet S, Garnero L (1997). A Bayesian approach to introducing anatomo-functional priors in the EEG/MEG inverse problem. *IEEE Trans Biomed Eng* 44: 374–385.

Baillet S, Mosher J, Leahy R (2001). Electromagnetic brain mapping. *IEEE Sig Proc Mag* 18: 14–30.

Barkley GL, Moran JE, Takanashi Y, Tepley N (1991). Techniques for DC Magnetoencephalography. *J Clin Neurophysiol* 8: 189–199.

Barth D, Sutherling W, Engel J, Beatty J (1982). Neuromagnetic localization of epileptiform spike activity in the human brain. *Science* 218: 891–894.

Baumann SB, Wozny DR, Kelly SK, Meno FM (1997). The electrical conductivity of human cerebrospinal fluid at body temperature. *IEEE Trans Biomed Eng* 44: 220–223.

Bragin A, Engel J, Wilson CL, Fried I, Buzsáki G (1999). High-frequency oscillations in human brain. *Hippocampus* 9: 137–142.

Buiatti M, Peña M, Dehaene-Lambertz G (2009). Investigating the neural correlates of

continuous speech computation with frequency-tagged neuroelectric responses. *Neuroimage* 44: 509–519.

Cohen D (1968). Magnetoencephalography: Evidence of magnetic fields produced by alpha-rhythm currents. *Science* 161: 784–786.

Cohen D (1972). Magnetoencephalography: Detection of the brain's electrical activity with a superconducting magnetometer. *Science* 175: 664–666.

Cohen D, Palti Y, Cuffin BN, Schmid SJ (1980). Magnetic fields produced by steady currents in the body. *Proc Natl Acad Sci U S A* 77: 1447–1451.

Collins DL, Neelin P, Peters TM, Evans AC (1994). Automatic 3D intersubject registration of MR volumetric data in standardized Talairach space. *J Comput Assist Tomogr* 18: 192–205.

Crick F, Koch C (1995). Are we aware of neural activity in primary visual cortex? *Nature* 375: 121–123.

Curio G, Mackert BM, Burghoff M, Koetitz R, Abraham-Fuchs K, Härer W (1994). Localization of evoked neuromagnetic 600 Hz activity in the cerebral somatosensory system. *Electroencephalogr Clin Neurophysiol* 91: 483–487.

Dale AM, Liu AK, Fischl BR, Buckner RL, Belliveau JW, Lewine JD, Halgren E (2000). Dynamic statistical parametric mapping: combining fMRI and MEG for high-resolution imaging of cortical activity. *Neuron* 26: 55–67.

Dale AM, Sereno MI (1993). Improved localization of cortical activity by combining EEG and MEG with MRI cortical surface reconstruction: A linear approach. *J Cogn Neurosci* 5: 162–176.

Daubechies I (1988). Orthonormal bases of compactly supported wavelets. *Comm Pure Appl Math* 41: 909–996.

De Tiège X, Op de Beeck M, Funke M, Legros B, Parkkonen L, Goldman S, Van Bogaert P (2008). Recording epileptic activity with MEG in a light-weight magnetic shield. *Epilepsy Res* 82: 227–231.

Enatsu R, Mikuni N, Usui K, Matsubayashi J, Taki J, Begum T, Matsumoto R, Ikeda A, Nagamine T, Fukuyama H, Hashimoto N (2008). Usefulness of MEG magnetometer for spike detection in patients with mesial temporal epileptic focus. *Neuroimage* 41: 1206–1219.

Engel AK, Fries P, Singer W (2001). Dynamic predictions: oscillations and synchrony in top-down processing. *Nat Rev Neurosci* 2: 704–716.

Engel AK, Singer W (2001). Temporal binding and the neural correlates of sensory awareness. *Trends Cogn Sci* 5: 16–25.

Erné SN, Scheer HJ, Hoke M, Pantev C, Lütkenhöner B (1987). Brainstem auditory evoked magnetic fields in response to stimulation with brief tone pulses. *Int J Neurosci* 37: 115–25.

Fischl B, Liu A, Dale AM (2001). Automated manifold surgery: constructing geometrically accurate and topologically correct models of the human cerebral cortex. *IEEE*

Trans Med Imaging 20: 70–80.

Fischl B, Salat DH, van der Kouwe AJW, Makris N, Ségonne F, Quinn BT, Dale AM (2004). Sequence-independent segmentation of magnetic resonance images. *Neuroimage* 23(Suppl 1): S69–S84.

Fischl B, Sereno MI, Tootell RB, Dale AM (1999). High-resolution intersubject averaging and a coordinate system for the cortical surface. *Hum Brain Mapp* 8: 272–284.

Friston K (2005). A theory of cortical responses. *Philos Trans R Soc Lond B Biol Sci* 360: 815–836.

Fujiki N, Jousmäki V, Hari R (2002). Neuromagnetic responses to frequency-tagged sounds: a new method to follow inputs from each ear to the human auditory cortex during binaural hearing. *J Neurosci* 22: RC205.

Furey ML, Tanskanen T, Beauchamp MS, Avikainen S, Uutela K, Hari R, Haxby JV (2006). Dissociation of face-selective cortical responses by attention. *Proc Natl Acad Sci U S A* 103: 1065–1070.

Gabor D (1946). Theory of communication. *J Inst Elec Eng* 93: 429–457.

Geselowitz DB (1970). On the magnetic field generated outside an inhomogeneous volume conductor by internal current sources. *IEEE Trans Magn* MAG-6: 346–347.

Giraud AL, Truy E, Frackowiak RS, Grégoire MC, Pujol JF, Collet L (2000). Differential recruitment of the speech processing system in healthy subjects and rehabilitated cochlear implant patients. *Brain* 123(Pt 7): 1391–1402.

Hari R (1990). The neuromagnetic method in the study of the human auditory cortex. In: Grandori F, Hoke M, Romani GL (eds.), *Auditory Evoked Magnetic Fields and Electric Potentials*, pp. 222–282. Karger, Basel.

Hari R, Forss N (1999). Magnetoencephalography in the study of human somatosensory cortical processing. *Philos Trans R Soc Lond B Biol Sci* 354: 1145–1154.

Hari R, Hällström J, Tiihonen J, Joutsiniemi SL (1989). Multichannel detection of magnetic compound action fields of median and ulnar nerves. *Electroencephalogr Clin Neurophysiol* 72: 277–280.

Hari R, Nishitani N (2004). From viewing of movement to imitation and understanding of other persons' acts: MEG studies of the human mirror-neuron system. In: Kanwisher N, Duncan J (eds.), *Functional Neuroimaging of Visual Cognition*, 1st ed., pp. 463–479. Oxford University Press, USA.

Hari R, Salmelin R (1997). Human cortical oscillations: a neuromagnetic view through the skull. *Trends Neurosci* 20: 44–49.

Hashimoto I, Mashiko T, Imada T (1996). Somatic evoked high-frequency magnetic oscillations reflect activity of inhibitory interneurons in the human somatosensory cortex. *Electroencephalogr Clin Neurophysiol* 100: 189–203.

Helenius P, Salmelin R, Service E, Connolly JF (1998). Distinct time courses of word and context comprehension in the left temporal cortex. *Brain* 121 (Pt 6): 1133–1142.

Hillebrand A, Barnes GR (2002). A quantitative assessment of the sensitivity of whole-

head MEG to activity in the adult human cortex. *Neuroimage* 16: 638–650.

Huang M, Dale AM, Song T, Halgren E, Harrington DL, Podgorny I, Canive JM, Lewis S, Lee RR (2006). Vector-based spatial-temporal minimum L1-norm solution for MEG. *Neuroimage* 31: 1025–1037.

Hyvärinen A, Oja E (2000). Independent component analysis: algorithms and applications. *Neural Netw* 13: 411–430.

Hämäläinen M, Hari R (2002). Magnetoencephalographic characterization of dynamic brain activation: Basic principles and methods of data collection and source analysis. In: Toga AW, Mazziotta JC (eds.), *Brain Mapping: The Methods*, 2nd ed., pp. 227–253. Academic Press, San Diego.

Hämäläinen M, Hari R, Ilmoniemi RJ, Knuutila J, Lounasmaa OV (1993). Magnetoencephalography—theory, instrumentation, and applications to noninvasive studies of the working human brain. *Rev Mod Phys* 65: 413–497.

Hämäläinen M, Sarvas J (1989). Realistic conductivity geometry model of the human head for interpretation of neuromagnetic data. *IEEE Trans Biomed Eng* 36: 165–171.

Hämäläinen MS, Ilmoniemi RJ (1984). Interpreting measured magnetic fields of the brain: Estimates of current distributions. Tech. Rep. TKK-F-A559, Helsinki University of Technology.

Hämäläinen MS, Ilmoniemi RJ (1994). Interpreting magnetic fields of the brain: minimum norm estimates. *Med Biol Eng Comput* 32: 35–42.

Iramina K, Ueno S (1995). Measurement of brain-stem auditory-evoked magnetic fields using a highly sensitive SQUID magnetometer with a variable base-line. *IEEE Trans Magn* 31: 4271–4273.

Iwasaki M, Pestana E, Burgess RC, Lüders HO, Shamoto H, Nakasato N (2005). Detection of epileptiform activity by human interpreters: blinded comparison between electroencephalography and magnetoencephalography. *Epilepsia* 46: 59–68.

Jacobs J, Levan P, Châtillon C, Olivier A, Dubeau F, Gotman J (2009). High frequency oscillations in intracranial EEGs mark epileptogenicity rather than lesion type. *Brain* 132: 1022–1037.

Jewett DL, Romano MN, Williston JS (1970). Human auditory evoked potentials: Possible brain stem components detected on the scalp. *Science* 167: 1517–1518.

Josephson BD (1962). Possible new effects in superconductive tunnelling. *Phys Lett* 1: 251–253.

Kandel E, Schwartz J, Jessell T (2000). *Principles of Neural Science*. 4th ed. McGraw-Hill Medical, New York.

Kaneko K, Fujiki N, Hari R (2003). Binaural interaction in the human auditory cortex revealed by neuromagnetic frequency tagging: no effect of stimulus intensity. *Hear Res* 183: 1–6.

Kelhä VO, Pukki JM, Peltonen RS, Penttinen AJ, Ilmoniemi RJ, Heino JJ (1982). Design, construction, and performance of a large-volume magnetic shield. *IEEE Trans Magn*

MAG-18: 260–270.

Kleinschmidt A, Büchel C, Zeki S, Frackowiak RS (1998). Human brain activity during spontaneously reversing perception of ambiguous figures. *Proc Biol Sci* 265: 2427–2433.

Kutas M, Hillyard SA (1980). Reading senseless sentences: Brain potentials reflect semantic incongruity. *Science* 207: 203–205.

Lachaux JP, Rodriguez E, Martinerie J, Varela FJ (1999). Measuring phase synchrony in brain signals. *Hum Brain Mapp* 8: 194–208.

Lamme VA (1995). The neurophysiology of figure-ground segregation in primary visual cortex. *J Neurosci* 15: 1605–1615.

Lammertmann C, Lütkenhöner B (2001). Near-DC magnetic fields following a periodic presentation of long-duration tonebursts. *Clin Neurophysiol* 112: 499–513.

Lansing RW (1964). Electroencephalographic correlates of binocular rivalry in man. *Science* 146: 1325–1327.

Latikka J, Kuurne T, Eskola H (2001). Conductivity of living intracranial tissues. *Phys Med Biol* 46: 1611–1616.

Lee TS, Mumford D (2003). Hierarchical Bayesian inference in the visual cortex. *J Opt Soc Am A Opt Image Sci Vis* 20: 1434–1448.

Leopold DA, Logothetis NK (1999). Multistable phenomena: changing views in perception. *Trends Cogn Sci* 3: 254–264.

Leopold DA, Wilke M, Maier A, Logothetis NK (2002). Stable perception of visually ambiguous patterns. *Nat Neurosci* 5: 605–609.

Liljeström M, Hultén A, Parkkonen L, Salmelin R (2009). Comparing MEG and fMRI views to naming actions and objects. *Hum Brain Mapp* 30: 1845–1856.

Liu AK, Belliveau JW, Dale AM (1998). Spatiotemporal imaging of human brain activity using functional MRI constrained magnetoencephalography data: Monte Carlo simulations. *Proc Natl Acad Sci U S A* 95: 8945–8950.

Longtin A, Bulsara A, Moss F (1991). Time-interval sequences in bistable systems and the noise-induced transmission of information by sensory neurons. *Phys Rev Lett* 67: 656–659.

Lu Z, Kaufman L (eds.) (2003). *Magnetic Source Imaging of the Human Brain*. 1st ed. Lawrence Erlbaum, Mahwah.

Lumer ED, Friston KJ, Rees G (1998). Neural correlates of perceptual rivalry in the human brain. *Science* 280: 1930–1934.

Lütkenhöner B, Lammertmann C, Ross B, Pantev C (2000). Brain stem auditory evoked fields in response to clicks. *Neuroreport* 11: 913–918.

Mackert BM, Wübbeler G, Leistner S, Trahms L, Curio G (2001). Non-invasive single-trial monitoring of human movement-related brain activation based on DC-magnetoencephalography. *Neuroreport* 12: 1689–1692.

Mahler R (2003). Multitarget Bayes filtering via first-order multitarget moments. *IEEE*

Trans Aerospace Elec Syst 39: 1152–1178.

Markand ON, Farlow MR, Stevens JC, Edwards MK (1989). Brain-stem auditory evoked potential abnormalities with unilateral brain-stem lesions demonstrated by magnetic resonance imaging. *Arch Neurol* 46: 295–299.

Matsuura K, Okabe Y (1995). Selective minimum-norm solution of the biomagnetic inverse problem. *IEEE Trans Biomed Eng* 42: 608–615.

Morlet J, Arens G, Fourgeau E, Giard D (1982). Wave propagation and sampling theory – Part I: Complex signal and scattering in multilayered media. *Geophys* 47: 203–221.

Mosher J, Lewis P, Leahy R (1992). Multiple dipole modeling and localization from spatio-temporal MEG data. *IEEE Trans Biomed Eng* 39: 541–557.

Mosher JC, Baillet S, Leahy RM (1999). EEG source localization and imaging using multiple signal classification approaches. *J Clin Neurophysiol* 16: 225–238.

Moss F, Ward LM, Sannita WG (2004). Stochastic resonance and sensory information processing: a tutorial and review of application. *Clin Neurophysiol* 115: 267–281.

Mountcastle VB (1998). *Perceptual Neuroscience: The Cerebral Cortex*. 1st ed. Harvard University Press, Cambridge.

Murakami S, Okada Y (2006). Contributions of principal neocortical neurons to magnetoencephalography and electroencephalography signals. *J Physiol* 575: 925–936.

Mäkelä JP, Forss N, Jääskeläinen J, Kirveskari E, Korvenoja A, Paetau R (2006). Magnetoencephalography in neurosurgery. *Neurosurgery* 59: 493–511.

Møller A (2007). Neural generators for auditory brainstem evoked potentials. In: Burkard RF, Don M, Eggermont JJ (eds.), *Auditory Evoked Potentials: Basic Principles and Clinical Application*, 1st ed., pp. 336–354. Lippincott Williams & Wilkins, Baltimore.

Näätänen R, Ilmoniemi RJ, Alho K (1994). Magnetoencephalography in studies of human cognitive brain function. *Trends Neurosci* 17: 389–395.

Okada YC (1982). Neurogenesis of evoked magnetic fields. In: Williamson SJ, Romani GL, Kaufman L, Modena I (eds.), *Biomagnetism: An Interdisciplinary Approach*, pp. 399–408. Plenum Press, New York.

Ou W, Hämäläinen MS, Golland P (2009). A distributed spatio-temporal EEG/MEG inverse solver. *Neuroimage* 44: 932–946.

Parkkonen LT, Simola JT, Tuoriniemi JT, Ahonen AI (1999). An interference suppression system for multichannel magnetic field detector arrays. In: Yoshimoto T, Kotani M, Kuriki S, Karibe H, Nakasato N (eds.), *Recent Advances in Biomagnetism*, pp. 13–16. Tohoku University Press, Sendai.

Pascarella A, Sorrentino A, Piana M, Parkkonen L (2007). Particle filters and RAP-MUSIC in MEG source modelling: A comparison. *Proc 15th Intl Conf Biomagn; Intl Congr Ser* 1300: 161–164.

Pitts MA, Gavin WJ, Nerger JL (2008). Early top-down influences on bistable perception revealed by event-related potentials. *Brain Cogn* 67: 11–24.

Plonsey R (1969). *Bioelectric Phenomena*. McGraw-Hill, New York.

Purves D, Augustine GJ, Fitzpatrick D, Hall WC, Lamantia A, McNamara JO, Williams SM (2004). *Neuroscience*. 3rd ed. Sinauer Associates, Sunderland.

Roland PE, Zilles K (1996). The developing European computerized human brain database for all imaging modalities. *Neuroimage* 4: S39–S47.

Saalmann YB, Pigarev IN, Vidyasagar TR (2007). Neural mechanisms of visual attention: how top-down feedback highlights relevant locations. *Science* 316: 1612–1615.

Salmelin R (2007). Clinical neurophysiology of language: the MEG approach. *Clin Neurophysiol* 118: 237–254.

Sarvas J (1987). Basic mathematical and electromagnetic concepts of the biomagnetic inverse problem. *Phys Med Biol* 32: 11–22.

Scherg M, von Cramon D (1985). Two bilateral sources of the late AEP as identified by a spatio-temporal dipole model. *Electroenceph Clin Neurophysiol* 62: 32–44.

Schmidt RO (1986). Multiple emitter location and signal parameter estimation. *IEEE Trans Antennas Propagat* AP-34: 276–280.

Schormann T, Henn S, Zilles K (1996). A new approach to fast elastic alignment with applications to human brains. In: Höhne KH, Kikinis R (eds.), *Visualization in Biomedical Computing*, pp. 337–342. Springer, Berlin.

Sinkkonen J, Tiitinen H, Näätänen R (1995). Gabor filters: an informative way for analysing event-related brain activity. *J Neurosci Methods* 56: 99–104.

Srinivasan R, Russell DP, Edelman GM, Tononi G (1999). Increased synchronization of neuromagnetic responses during conscious perception. *J Neurosci* 19: 5435–5448.

Stenbacka L, Vanni S, Uutela K, Hari R (2002). Comparison of minimum current estimate and dipole modeling in the analysis of simulated activity in the human visual cortices. *Neuroimage* 16: 936–943.

Sterzer P, Rees G (2008). A neural basis for percept stabilization in binocular rivalry. *J Cogn Neurosci* 20: 389–399.

Sutter EE (2001). Imaging visual function with the multifocal m-sequence technique. *Vision Res* 41: 1241–1255.

Talairach J, Tournoux P (1988). *Co-Planar Stereotaxic Atlas of the Human Brain: 3-D Proportional System: An Approach to Cerebral Imaging*. Georg Thieme Verlag, Stuttgart.

Tallon-Baudry C, Bertrand O, Delpuech C, Pernier J (1996). Stimulus specificity of phase-locked and non-phase-locked 40 Hz visual responses in human. *J Neurosci* 16: 4240–4249.

Tallon-Baudry C, Bertrand O, Delpuech C, Pernier J (1997). Oscillatory gamma-band (30–70 Hz) activity induced by a visual search task in humans. *J Neurosci* 17: 722–734.

Tanskanen T, Näsänen R, Ojanpää H, Hari R (2007). Face recognition and cortical responses: effect of stimulus duration. *Neuroimage* 35: 1636–1644.

Tarkiainen A, Helenius P, Hansen PC, Cornelissen PL, Salmelin R (1999). Dynamics

of letter string perception in the human occipitotemporal cortex. *Brain* 122 (Pt 11): 2119–2132.

Taulu S, Kajola M (2005). Presentation of electromagnetic multichannel data: The signal space separation method. *J Appl Phys* 97: 124905–124910.

Tesche CD (1996). Non-invasive imaging of neuronal population dynamics in human thalamus. *Brain Res* 729: 253–258.

Tesche CD, Uusitalo MA, Ilmoniemi RJ, Huotilainen M, Kajola M, Salonen O (1995). Signal-space projections of MEG data characterize both distributed and well-localized neuronal sources. *Electroencephalogr Clin Neurophysiol* 95: 189–200.

Tononi G, Srinivasan R, Russell DP, Edelman GM (1998). Investigating neural correlates of conscious perception by frequency-tagged neuromagnetic responses. *Proc Natl Acad Sci U S A* 95: 3198–3203.

Tripp JH (1981). Biomagnetic fields and cellular current flow. In: Erné SN, Hahlbohm HD, Lübbig H (eds.), *Biomagnetism*, pp. 207–215. Walter de Gruyter, Berlin.

Uusitalo M, Ilmoniemi R (1997). Signal-space projection method for separating MEG or EEG into components. *Med Biol Eng Comput* 35: 135–140.

Uusitalo MA, Williamson SJ, Seppä MT (1996). Dynamical organisation of the human visual system revealed by lifetimes of activation traces. *Neurosci Lett* 213: 149–152.

Uutela K, Hämäläinen M, Somersalo E (1999). Visualization of magnetoencephalographic data using minimum current estimates. *Neuroimage* 10: 173–180.

Uutela K, Taulu S, Hämäläinen M (2001). Detecting and correcting for head movements in neuromagnetic measurements. *Neuroimage* 14: 1424–1431.

Vanhatalo S, Palva JM, Holmes MD, Miller JW, Voipio J, Kaila K (2004). Infraslow oscillations modulate excitability and interictal epileptic activity in the human cortex during sleep. *Proc Natl Acad Sci U S A* 101: 5053–5057.

Vanni S, Henriksson L, James AC (2005). Multifocal fMRI mapping of visual cortical areas. *Neuroimage* 27: 95–105.

Varela F, Lachaux JP, Rodriguez E, Martinerie J (2001). The brainweb: phase synchronization and large-scale integration. *Nat Rev Neurosci* 2: 229–239.

Varpula T, Poutanen T (1984). Magnetic field fluctuations arising from thermal motion of electric charge in conductors. *J Appl Phys* 55: 4015–4021.

von der Malsburg C (1999). The what and why of binding: the modeler's perspective. *Neuron* 24: 95–104, 111–125.

Vrba J, Robinson SE (2001). Signal processing in magnetoencephalography. *Methods* 25: 249–71.

Vvedensky V, Hari R, Ilmoniemi R, Reinikainen K (1985). Physical basis of neuromagnetic fields. *Biophysica* 30: 154–158.

Windmann S, Wehrmann M, Calabrese P, Güntürkün O (2006). Role of the prefrontal cortex in attentional control over bistable vision. *J Cogn Neurosci* 18: 456–471.

Wolters CH, Anwander A, Tricoche X, Weinstein D, Koch MA, MacLeod RS (2006).

Influence of tissue conductivity anisotropy on EEG/MEG field and return current computation in a realistic head model: a simulation and visualization study using high-resolution finite element modeling. *Neuroimage* 30: 813–826.

Woods RP, Grafton ST, Watson JD, Sicotte NL, Mazziotta JC (1998). Automated image registration: II. Intersubject validation of linear and nonlinear models. *J Comput Assist Tomogr* 22: 153–165.

Zappia M, Cheek JC, Lüders H (1996). Brain-stem auditory evoked potentials (BAEPs) from basal surface of temporal lobe recorded from chronic subdural electrodes. *Electroencephalogr Clin Neurophysiol* 100: 141–151.

Zimmerman JE, Thiene P, Harding JT (1970). Design and operation of stable rf-biased superconducting point-contact quantum devices and a note on the properties of perfectly clean metal contacts. *J Appl Phys* 41: 1572–1580.

ISBN 978-951-22-9950-8
ISBN 978-951-22-9951-5 (PDF)
ISSN 1795-2239
ISSN 1795-4584 (PDF)